

Characterization of the Crab Pulsar’s Timing Noise

D. M. Scott ¹, M. H. Finger ¹ and C. A. Wilson

National Space Science and Technology Center, Huntsville, AL 35805

Matthew.Scott@nsstc.nasa.gov

ABSTRACT

We present a power spectral analysis of the Crab pulsar’s timing noise, mainly using radio measurements from Jodrell Bank taken over the period 1982-1989, an interval bounded by sparse data sampling and a large glitch. The power spectral analysis is complicated by nonuniform data sampling and the presence of a steep red power spectrum that can distort power spectra measurement by causing severe power “leakage”. We develop a simple windowing method for computing red noise power spectra of uniformly sampled data sets and test it on Monte Carlo generated sample realizations of red power-law noise. We generalize time-domain methods of generating power-law red noise with even integer spectral indices to the case of noninteger spectral indices. The Jodrell Bank pulse phase residuals are dense and smooth enough that an interpolation onto a uniform time series is possible. A windowed power spectrum is computed revealing a periodic or nearly periodic component with a period of 568 ± 10 days and a $1/f^3$ power-law noise component in pulse phase with a noise strength $S_\phi = (1.24 \pm 0.067) \times 10^{-16}$ cycles²/sec² over the analysis frequency range $f = 0.003 - 0.1$ cycles/day. This result deviates from past analyses which characterized the pulse phase timing residuals as either $1/f^4$ power-law noise or a quasiperiodic process. The analysis was checked using the Deeter polynomial method of power spectrum estimation that was developed for the case of nonuniform sampling, but has lower spectral resolution. The timing noise is consistent with a torque noise spectrum rising with analysis frequency as f implying *blue* torque noise, a result not predicted by current models of pulsar timing noise. If the periodic or nearly periodic component is due to a binary companion, we find a mass function $f(M) = (6.8 \pm 2.4) \times 10^{-16} M_\odot$ and a companion mass, $M_c \geq 3.2M_\oplus$ assuming a Crab pulsar mass of $1.4M_\odot$.

Key words: pulsars:individual(Crab pulsar) — methods:statistical — stars:oscillations.

¹Universities Space Research Association

Submitted to MNRAS 10/30/2002

1. Introduction

Isolated rotation-powered pulsars generally exhibit a pulse frequency that can be measured to high precision and that decreases, for the most part smoothly, on long time scales, indicating a steady loss of angular momentum from the rotating neutron star. The deterministic spindown trend of the pulsars can be modeled by a low order polynomial in the pulse phase. Apart from well known “glitches” in rotation rate occasionally observed in a few pulsars, many pulsars show fluctuations in the pulse phase about the deterministic trend. These rotation fluctuations or “timing noise”, often do not have the form of white noise but rather exhibit a “wandering” behavior with a roughly polynomial appearance. This is not a sign of unmodeled higher order polynomial terms in the deterministic spindown trend, however, since adding more polynomial terms does not improve one’s ability to predict the pulse phase. The nature of these rotation fluctuations is of interest since they provide direct observational information on the forces acting upon the neutron star crust. The presence of timing noise also complicates the detection of perturbations to the pulse phase caused by orbiting neutron star companions and has the potential to be mistaken for such perturbations if not properly understood.

The Crab pulsar spins at a rotation frequency of 30 Hz and is the most well observed of all isolated pulsars. The Crab pulsar was first discovered in 1968 and has been subjected to many long term observation programs at optical and radio wavelengths (Groth 1975a; Gullahorn et al. 1977; Lohsen 1981; Lyne, Pritchard & Smith 1988, 1993). There have been several prior analyses of the long term properties of the pulse phase of the Crab pulsar. They all agree that the intrinsic pulse phase can be divided into three components: (1) A long term spin down that can be characterized by a low order polynomial (2) several glitches and (3) timing noise.

The nature of the Crab timing noise has been investigated a number of times. The timing noise is revealed as the dominant component in the timing residuals after removal of a spindown polynomial and glitches from the pulse phase. The timing residuals from optical observations were compared to noise models consisting of random walks in pulse phase, pulse frequency or pulse frequency derivative (Boynton et al. 1972; Groth 1975b,c; Cordes 1980) and found to be most consistent with a random walk in pulse frequency in all cases. A low resolution power spectrum was calculated for the pulse frequency derivative using a polynomial estimator method by Deeter (1981) (also displayed in Boynton 1981; Alpar, Nandkumar & Pines 1986), who found a white spectrum consistent with a random

walk in pulse frequency. For a review of this work see D’Alessandro (1997) and Deshpande et al. (1996). In contrast, using a five year span of radio observations from Jodrell Bank in the 1980’s, Lyne, Pritchard & Smith (1988) claimed that the timing residuals were consistent with a physically real quasiperiodic process with a period of ~ 20 months since the period did not scale with the length of the data being fit, as occurs with the apparent periods observed in the residuals of polynomial fits to red noise. The disagreement between these various analyses has motivated this study of the timing properties of the Crab pulsar and a search for analysis techniques to better characterize the statistical nature of the timing noise.

We focus on power spectral analysis methods in this paper to characterize the Crab pulsar timing residuals. The power spectral analysis is not straightforward due to a steep rise in power at low analysis frequencies and due to the nonuniform sampling of the data sets. The Crab timing residuals most likely contain some type of red power-law noise process, of which the random walk is a well-known example. Random walks have power spectra that rise as $1/f^2$ toward low analysis frequencies (f). We will refer to f as *analysis* frequency to prevent confusion with the *pulse* frequency ν . In general, a steep rise in power at low analysis frequencies can cause severe power “leakage” into the low frequency side-lobes of the frequency response of power spectral estimators, such as the squared amplitudes of a Fourier transform, that can be comparable to or greater than the response at the nominal frequency of the estimator itself. The leaked power greatly distorts the computed power spectrum preventing detection of its true form unless special precautions are taken to control this leakage.

The nonuniformity of sampling has been severe in the pulse timing data sets obtained from optical observation programs that were carried out during the interval from 1969 to 1980. The optical observations are subject to seasonal and monthly interruptions due to conjunctions of the Crab pulsar with the sun and moon. The total length of a data set that can be analyzed using a single pulse phase ephemeris has been limited as well due to the occurrence of occasional large glitches that hinder correct extrapolation of the pulse phase across the glitch. Long term radio monitoring of the Crab pulsar at Jodrell Bank from 1982 to the present has produced a set of pulse arrival times with much smaller gaps than in the optical data and generally has a higher sampling rate. In this paper we concentrate on a subset of the Jodrell Bank data set over the 7.5 year interval from February 1982 to August 1989 that is bounded by sparse data sampling prior to 1982 and a large glitch that occurred in 1989.

Mathematical characterization of the timing noise in the Crab and other pulsars has frequently been in terms of red power-law noise processes that consist of random walks

in the pulse phase, pulse frequency or pulse frequency derivative or mixtures thereof (e.g Cordes and Downs 1985). One of the major attractions of these models is that discrete random walk realizations (and summations thereof) can be easily generated numerically using time domain methods. Random walks and their repeated summations (or integrals in the case of continuous sampling) all have ensemble averaged power spectra of the form $1/f^m$ where the power-law spectral index m is an even integer. These noise models have been important for checking and calibrating various red noise analysis methods. We show that these time domain methods can be generalized to produce red-power law noise processes with arbitrary spectral indices (see appendix A). In addition, red (and blue) power law noise realizations with arbitrary spectral indices can also be generated using frequency domain methods. We use both time domain and frequency domain simulated noise realizations to check the accuracy, efficacy and calibration of the analysis procedures used in this study.

Analysis of pulse arrival times necessarily requires the fitting of a low order polynomial to obtain timing residuals. When the timing noise has a steep red power spectrum, the polynomial fitting removes noise power at the lowest frequencies, creating a low frequency turnover or peak in the power spectrum. In the time domain, this tends to produce residuals with a quasiperiodic appearance. The appearance of a low frequency quasiperiodic looking residue can easily be mistaken for a real quasiperiodicity or even a real periodicity by the unwary investigator when in fact the quasiperiodicity is purely an artifact of the polynomial fitting and the quasiperiod will scale with the length of the data fit. To detect a true low-frequency quasiperiodicity in the presence of detrended red noise requires more careful analysis than simple visual inspection of the timing residuals. We show that in the Crab pulsar, a real periodicity or quasiperiodicity is present in the power spectrum of the Crab timing residuals produced from the Jodrell Bank observations in addition to a red noise component.

The analysis of Deeter (1981) involved developing and applying a method of computing low frequency resolution power spectra that deals with the problems of nonuniform sampling and red noise leakage. The method uses polynomial fits on a hierarchy of time scales to generate a power spectrum at octave frequency resolution. The low frequency resolution of this method means that any significant narrow features in the power spectrum will be unresolved and allows significant room for misinterpretation of the power spectral shape. We show that high resolution power spectra can be computed for the case of uniform data sampling by use of a simple windowing procedure in conjunction with polynomial detrending to alleviate the leakage problem. The smoothness and dense sampling of the Crab timing residuals produced from the Jodrell Bank observations makes possible an interpolation onto a uniform grid and computation of a high resolution power spectrum. This new analysis shows that the pulse phase timing noise is composed of two components: a red noise process

with an approximately $1/f^3$ power density spectrum and a long term periodic or nearly periodic oscillation with a period of 568 ± 10 days. We confirm this result, at lower spectral resolution, using the Deeter polynomial method.

2. The major components of the pulse phase of the Crab pulsar

The pulse phase of the Crab pulsar is obtained via the application of a pulse phase ephemeris to a set of measured pulse arrival times that have been corrected to the solar system barycenter and corrected for other timing delays such as those caused by interstellar dispersion of radio waves (see Lyne, Pritchard & Smith, 1988). For the Crab pulsar, the intrinsic pulse phase can be decomposed conceptually into three components: 1) the pulsar spin frequency and its deterministic decrease, 2) glitches and 3) rotation fluctuations about the deterministic trend. These appear to be essentially independent components although the presence of glitches may be effecting the long term slow-down process (Lyne, Pritchard & Smith, 1993). In addition, we will consider the possible presence of a longterm quasiperiodic or periodic variation in the pulse phase. The pulse phase can be represented by a model:

$$\phi(t) = \phi_S(t) + \phi_G(t) + \phi_{TN}(t) + \phi_{QP}(t) + \phi_M(t) \quad (1)$$

representing respectively the contributions of the rotation frequency and its deterministic spindown (ϕ_S), glitches (ϕ_G), intrinsic timing noise (ϕ_{TN}), a quasiperiodic process (ϕ_{QP}) and measurement errors (ϕ_M). In order to study the properties or detect the presence of any random or longterm periodic processes in the pulse phase we have to investigate the properties of the pulse phase residuals $\phi_{res}(t) = \phi(t) - \phi_{eph}(t)$ on a time span T rather than $\phi(t)$ directly. The pulse phase ephemeris usually consists only of a low order polynomial to model ϕ_S , although “glitch functions” are sometimes added to fit the glitches. For the data sets analyzed in this paper, glitches will either be absent or only a minor perturbation on the pulse phase residuals that remains after subtraction of the pulse phase ephemeris.

The deterministic spindown of the Crab pulsar is modeled using a simple spindown model, $\dot{\nu} = -K\nu^n$, where ν is the rotation frequency and n is the braking index. The value of the braking index depends on the mechanism slowing down the pulsar. For braking purely by the emission of magnetic dipole radiation $n = 3$ and for braking only by emission of a wind $n = 1$. The braking index can be determined using $n = \frac{\nu_0 \ddot{\nu}_0}{\dot{\nu}_0^2}$ if $\ddot{\nu}_0$ can be measured. The analytic solution to the spindown model is given by:

$$\phi_s(t - t_0) = \dot{\nu}_0^{-1} \nu_0^2 (2 - n)^{-1} \left(\left[1 + \dot{\nu}_0 \nu_0^{-1} (1 - n)(t - t_0) \right]^{\frac{(2-n)}{(1-n)}} - 1 \right) + \phi_0. \quad (2)$$

The term $\dot{\nu}_0 \nu_0^{-1}$ is quite small for all known pulsars so the analytic solution can be expanded

using the binomial theorem into a “spindown polynomial”:

$$\phi_s(t - t_0) = \phi_0 + \nu_0(t - t_0) + \frac{1}{2}\dot{\nu}_0(t - t_0)^2 + \frac{1}{6}\ddot{\nu}_0(t - t_0)^3 + \frac{1}{24}\ddot{\nu}_0(t - t_0)^4 \dots \quad (3)$$

The Crab pulsar has a measured pulse frequency derivative of $\dot{\nu}_0 = -3.862 \times 10^{-10}$ Hz/s and a braking index of 2.5 (Lyne, Pritchard & Smith 1993) thus successive coefficients in the Crab spindown polynomial will decrease in magnitude by a factor of $\approx 10^{-10}$. This implies that, if the rotation phase consisted only of this spindown polynomial, a polynomial fit of order l will always produce polynomial residuals of order $l + 1$, unless masked by measurement errors. The timing noise in the Crab pulsar was initially revealed by the presence of polynomial-like residuals that were much larger those expected from a pure spindown polynomial (Boynton et al. 1972).

3. Observations and computation of pulse timing residuals

A set of radio pulse arrival times for the Crab pulsar corrected to the solar-system barycenter were obtained from Jodrell Bank (Lyne, private communication). The data consist of 7177 arrival times collected over a nine year span from January 27, 1982 to January 23, 1991 (Truncated Julian Days 4996 to 8279; TJD = JD – 2440000.5) at five radio frequencies (408, 610, 930, 1420 and 1667 Mhz) with approximately 85% of the arrival times at 610 Mhz. The typical arrival time error was 9 microseconds. These data or portions thereof have been previously presented in Lyne and Pritchard (1987), Lyne, Pritchard & Smith (1988) and Lyne, Smith & Pritchard (1992) and Lyne, Pritchard & Smith (1993). Two glitches are present in the data occurring on TJD 6664 with a $\Delta\nu/\nu \sim 10^{-10}$ (Lyne and Pritchard 1987) and TJD 7767 (Lyne, Smith and Pritchard 1992). The second glitch is one of the largest reported for the Crab pulsar ($\Delta\nu/\nu \sim 10^{-9}$) and the post glitch arrival times are sufficiently distorted from their pre-glitch behavior that only data prior to this glitch were included in the subsequent analysis (4530 arrival times). In contrast, the glitch occurring on TJD 6664 was a relatively small event and is discussed in section 8.

A quartic polynomial phase model of the form given by equation 3 was removed from the arrival times using values given in table 1 and the method described on page 104 of Manchester and Taylor (1977). The errors in the parameters were determined by the method of fitting a quartic polynomial + sinusoid to the phase residuals determined from an initial phase ephemeris. See section 8 for a description of this process.

The power-law spindown model given by equation 2 predicts a value for $\ddot{\nu}_0$ of

$$\ddot{\nu}_0 = n(2n - 1)\dot{\nu}_0^3/\nu_0^2$$

$$= -6.2 \times 10^{-31} \text{ Hz s}^{-3} \quad (4)$$

which is approximately *half* the value in table 1. The phase contribution of the measured $\ddot{\nu}_0$ term is 129 cycles over a period of 2500 days, whereas the value predicted by the power-law spindown model would contribute 56 cycles. Hence $\ddot{\nu}_0$ should be easily measureable without much distortion caused by red noise interference. The secular spin-down thus appears to be somewhat more complex than that predicted by a simple power-law spin-down model. This may be an indication of the longterm effects on the spin down process caused by glitches (Lyne, Pritchard & Smith (1993)).

The arrival time data recieved from Jodrell Bank had been corrected only for a single value of the dispersion measure (DM) over the entire data span. Therefore, prior to removal of the quartic polynomial phase model, the arrival times were corrected using the difference between monthly DM measurements taken from the Crab pulsar monthly ephemeris available at the world wide website: <http://www.jb.man.ac.uk/pulsar/crab.html> and a single DM value of 56.743. The changes in the DM value from month-to-month caused small discontinuities in the arrival times at the bin boundaries. This problem was dealt with by making a cubic spline interpolation to the set of monthly DM values at a higher time resolution and then computing DM values with a linear interpolation at the actual data times using the nearest pair of DM values from the cubic spline interpolation. The resulting timing residuals are quite smooth and very similar to that displayed in figure 6 of Lyne, Pritchard & Smith (1993). A fair number of points (130) deviated significantly from the local trend in the timing residuals. These were judged to be outliers and removed. We show the timing residuals in the top panel of figure 1. The timing residuals are relatively smooth and display an apparent quasiperiodic process. The number of zero-crossings is ten, five more than expected if a pure spindown polynomial were present.

4. Red Power-law noise processes

The timing noise in the Crab pulsar has been attributed to a random walk in pulse frequency by several previous analyses (Boynton et al. 1972; Groth 1975b,c; Cordes 1980). A random walk is a member of the class of power-law noise processes and has an $1/f^2$ power-law power spectrum. In pulse phase, that is the integrated pulse frequency, the power spectrum steepens to a $1/f^4$ power-law. We will refer to these type of noise models as red power-law noise (PLN). The *a priori* knowledge that red PLN is probably present is important since analysis methods and interpretations that usually assume only white noise is present would produce erroneous results.

Random walks in pulse phase, pulse frequency and pulse frequency derivative² have been considerably investigated with respect to pulsar timing noise since these are simple models with which noise realizations can easily be generated. They are members of the class of red PLN processes with $1/f^m$ spectra where $m = 2, 4, 6, \dots$ that can be generated by repeated integration of white noise. Integration of white noise processes will produce random walks which have an ensemble averaged power density spectrum with a power-law spectral index of $m = 2$. Integration of the random walks will produce noise realizations with an ensemble averaged power-law spectral index of $m = 4$. The time series becomes smoother with each integration and hence “redder” in appearance as the low frequency components of the time series become more dominant. For example, a white noise process in the pulse frequency derivative will produce a random walk in pulse frequency and an integrated random walk in pulse phase. In general, each integration will increase the power-law index of the power density spectrum of the noise process by 2. To see this, consider a zero mean continuous³ white noise process, $\epsilon(t)$, with an autocovariance function $\langle \epsilon(t)\epsilon(t + \tau) \rangle = \sigma_\epsilon^2 \delta(\tau)$, where $\delta(t)$ is the Dirac delta-function. The quantity $S = \sigma_\epsilon^2$ is called the “noise strength” and is a fixed parameter that characterizes the white noise. The ensemble averaged power density per unit analysis frequency of $\epsilon(t)$ will be a constant, $\langle |F_\epsilon(f)|^2 \rangle = S$ where f is analysis frequency and $F_\epsilon(f)$ is the Fourier transform of $\epsilon(t)$. The derivative theorem for Fourier transforms states that: if $f(t)$ has a Fourier transform $F(f)$ then $f'(t)$ has a Fourier transform $i2\pi f F(f)$. Let us consider a random walk defined by:

$$r_2(t) = \int_{-\infty}^t \epsilon(t') dt' \quad (5)$$

where the subscript on $r(t)$ will refer to the power-law spectral index of the process which has a $1/f^2$ ensemble-averaged spectrum and the Fourier transform of $r_2(t)$ is $F_{r_2}(f)$. Since $\epsilon(t)$ is a continuous random process existing at all t on $-\infty < t < +\infty$, and $F_\epsilon(f)$ exists in the limit of the Fourier Transform of band-limited white noise, the fact that $r_2'(t) = \epsilon(t)$ implies that the Fourier transform of r_2' is $i2\pi f F_{r_2}(f)$ and is equal to $F_\epsilon(f)$. Therefore, $F_{r_2}(f) = F_\epsilon(f)/i2\pi f$. The ensemble averaged power density spectrum of $r_2(t)$ is defined by: $P_{r_2}(f) = P_\epsilon(f)/4\pi^2 f^2 = S/4\pi^2 f^2$. This argument can be repeated for each successive integration. Thus each integration will steepen the power density spectrum by a factor $1/(4\pi^2 f^2)$.

²Groth (1975b) refers to these respectively as “phase noise” (PN), “frequency noise” (FN) and “slowing-down noise” (SN), whereas Deeter (1984) refers to $1/f^m$ power-law noise with $m = 2, 4, 6$ as 1st, 2nd and 3rd order red noise respectively.

³Continuous in the random variable sense, i.e. defined for all times t

Previous timing analysis of the Crab pulsar (Boynton et al. 1972; Groth 1975b,c; Cordes 1980 and Deeter 1981) focused on power-law noise processes that could be generated by the integration or summation of white noise realizations and so was biased toward power-law noise processes with even integer spectral indices. There is no *a priori* reason that the timing noise should be restricted to an even integer red power-law noise process and a truly general analysis method should be able to tell the spectral index of any power-law noise directly rather than making a best fit from among a set of expected indices as has been done in several of these past analyses. The Deeter polynomial method (Deeter & Boynton 1982, Deeter 1984) can in principle determine the power-law index directly but has such low spectral resolution that the presence of any discrete features such as those due to a quasiperiodic process will produce an erroneous interpretation. A need exists for higher spectral resolution methods that can directly determine the power spectral index and distinguish the presence of narrow features, which we explore below.

In order to test possible analysis methods, we develop a time domain method to generate red power-law noise realizations with an arbitrary spectral index in Appendix A, which is a generalization of the discussion given by Groth (1975b). A useful, but unnormalized, frequency domain method which weights Fourier amplitudes by a power-law and then inverse Fourier transforms the result into the time domain has been presented by Timmer & König (1995) which also generates PLN realizations with an arbitrary spectral index and is very straightforward to implement (see Appendix B for a normalized method).

5. Power Spectral Density Estimation of Red Noise Processes

The estimation of the power density spectrum (PDS) of a red PLN realization presents special problems due to the steep power rise in the spectrum at low frequencies. The problem arises due to leakage of power in the low-frequency sidelobe of the frequency response of a spectral density estimator which can greatly exceed the response at the central or nominal frequency. Consider a noise realization $r_m(t)$ over the time interval $\frac{-T}{2}$ to $\frac{T}{2}$. The estimated PDS will be the squared modulus of the convolution the Fourier transform of the “window function”, $W(f)$ with the intrinsic Fourier transform of the noise process $F(f)$:

$$F_w(f) = \int_{-\infty}^{+\infty} F(f')W(f - f')df' \quad (6)$$

If the time interval extended over infinity then the Fourier transform of the window function would be a δ -function and the intrinsic power spectrum would be recovered exactly. The

ordinary rectangular window function:

$$w(t) = \begin{cases} 1 & \text{for } |t| \leq T/2 \\ 0 & \text{otherwise} \end{cases}$$

has a Fourier transform given by:

$$W(f) = \frac{\sin(\pi f T)}{\pi f}.$$

When $F(f)$ has a power-law form: $\frac{C}{(2\pi f)^m}$, the windowed Fourier transform is given by:

$$F_w(f) = \int_{-\infty}^{+\infty} \frac{C}{(\pi f')^m} \frac{\sin[\pi(f - f')T]}{2\pi(f - f')} df' \quad (7)$$

The power leakage problem occurs due to the singularity in the power-law noise spectrum at zero analysis frequency.

In practice, the rise in power towards zero frequency will exhibit a cut-off due to the use of a finite, rather than infinite, stretch of data. The main leakage problem is caused by the large, but finite power, at the lowest frequencies actually present. When $m \geq 2$, i.e. for red PLN as red or more red than a random walk, each frequency estimate will be dominated by the response to the power at the lowest frequencies. The estimated spectrum will then have a power-law spectral index of ≈ 2 regardless of the value of m . Detrending the data prior to power spectral estimation, by a polynomial fit for example, will decrease the power at the lowest frequencies and will help to alleviate the leakage problem irregardless of the type of power spectral estimator applied to the data with the tradeoff that the nondetrended form of the power spectrum cannot be measured directly. These issues will be further explored in section 7.

6. Computation of a Windowed PDS in the Presence of Red Power-Law Noise

A PDS of a uniformly sampled red noise time-series can be computed with fast Fourier Transforms by using an appropriate window function to control the power leakage. The window function must be chosen to sufficiently reduce the side-lobe response of the power density estimator (at the expense of spectral resolution) so that leakage is not a major problem. For a given time-series, $\{x_k, t_k\}$ $k = 0, 1, \dots, N - 1$, the Hamm window of the form $w_k = \sin^\alpha(\pi k/N)$ with $\alpha = 2$ has a frequency response with sidelobes whose envelope falls-off with analysis frequency as $\approx 1/f^6$ (see Harris 1985). This is sufficient for computation of power density spectra for red noise with power-law indices up to $m \approx 5$ according to the

moment condition criteria (Deeter & Boynton 1984). Presumably a window function could be designed to optimally suppress the side-lobe response while preserving maximum spectral resolution but this has not been pursued in this paper, since sine windows have proven to be simple and adequate in practice.

The actual method of PDS computation and normalization used here involves several steps. After a window, \hat{w}_k , is chosen the window is normalized to a root-mean square of 1:

$$w_k = \frac{\hat{w}_k}{\sqrt{\frac{1}{N} \sum_{k=0}^{N-1} \hat{w}_k^2}}$$

The PDS of $w_k x_k$ is computed as:

$$|\hat{a}_j|^2 = \left| \sum_{k=0}^{N-1} w_k x_k \exp(+2\pi i j k / N) \right|^2 \quad j = -\frac{N}{2}, \dots, \frac{N}{2} - 1$$

By taking advantage of the fact that for real data $|\hat{a}_j| = |\hat{a}_{-j}|$, the two-sided PDS is converted to a one-sided PDS, $|a_j|^2$, by doubling all powers except $|\hat{a}_0|^2$ and the Nyquist term ($|\hat{a}_{-N/2}|^2$) when N is even and eliminating all redundant negative frequency terms.

A normalization factor of $\frac{1}{2N}$ is applied to the $|a_j|^2$. This is done so that if x_k is a white noise process then the mean power level will equal the white noise variance. For example, if x_k is a white noise process with $\langle x_k^2 \rangle = \sigma_\epsilon^2$ and $\langle x_k \rangle = 0$ then:

$$\begin{aligned} \left\langle \sum_{k=0}^{N-1} |w_k x_k|^2 \right\rangle &= \sum_{k=0}^{N-1} w_k^2 \langle |x_k|^2 \rangle \\ &= \sigma_\epsilon^2 \sum_{k=0}^{N-1} w_k^2 \\ &= N \sigma_\epsilon^2 \end{aligned} \tag{8}$$

$$\tag{9}$$

Using Parseval's relation with the constant term ($j = 0$) deleted we have:

$$\begin{aligned} N \sigma_\epsilon^2 &= \frac{1}{N} \sum_{j=1}^{N/2} |a_j|^2 \\ &= \frac{1}{2} \bar{P} \end{aligned} \tag{10}$$

$$\tag{11}$$

where $|a_j|^2$ are the one-sided powers defined above and \bar{P} is the mean power level. We therefore define a normalized PDS as:

$$P_j = \frac{1}{2N} |a_j|^2 \quad j = 1, \dots, \frac{N}{2} \quad (12)$$

so the mean power level will approximately equal the white noise variance σ_ϵ^2 if x_k is a zero-mean white noise variable.

The power-law index of the red noise noise process can be determined by performing a linear fit to $\log P_j$ vs. $\log f_j$ where the $f_j = \frac{j}{N}$ are the analysis frequencies. An appropriate frequency range must be chosen for the fit to avoid frequency regions where the power spectrum contains substantial contributions from any other processes present in addition to a pure power-law noise process. In this paper we used linear least-squares fitting to estimate the slope. The data points $\log P_j$ do not have a gaussian distribution about a mean value $< \log P_j >$ as assumed in ordinary least-squares fitting, so some distortion in the slope and slope error estimates will be introduced. The actual distribution of the data points about a mean value is similar to gaussian but possesses a low value tail that results from taking the log of a chi-squared distribution with two degrees of freedom. The actual slope estimation procedure used here involved an initial fit with assumed unit errors on $\log P$, a calculation of the deviation of the fit residuals and then a new fit with uniform errors equal to the measured deviation. Monte Carlo simulations of this procedure on simulated data sets of 10000 sample realizations each for a variety of input power-law indices showed that no bias existed in the estimated mean slope value but the slope errors had been overestimated by a factor of 1.7. Hence, the slope errors quoted in this paper have been divided by 1.7.

The power density spectrum can be converted to a flattened form to allow clearer study of features unrelated to the power-law form. We chose a normalization that allows the noise strength to be estimated directly from the mean power-level over a suitable analysis frequency range. Given a power-law index m the power spectrum is multiplied by $(2\pi f_j)^m$. The analysis frequency is converted to physical units as $\nu_j = \left(\frac{f_j}{\Delta t}\right)$ where $\Delta t = t_{n+1} - t_n$. The flattened PDS is then normalized so the mean power level approximately equals the noise strength in physical units by multiplying by a factor $(\frac{1}{\Delta t})^{m-1}$. This is a combination of a factor of $(\frac{1}{\Delta t})^m$ to flatten the spectrum, a factor of $(\frac{1}{\Delta t})^{-2}$ to correct the power via the similarity theorem for the rescaling of the frequency and a factor of $(\frac{1}{\Delta t})$ to make the mean power level equal the noise strength in the presence of pure power-law noise. The extra factor of $(\frac{1}{\Delta t})$ arises from the definition of the noise strength S (see section 7 and Appendix A). The total set of operations on the one-sided PDS can be combined as:

$$P_{j,flattened} = \left(\frac{1}{2N}\right) (2\pi f_j)^m \left(\frac{1}{\Delta t}\right)^{m-1} |a_j|^2 \quad j = 1, \dots, \frac{N}{2} - 1. \quad (13)$$

Note that the power-law spectral index m is a free parameter supplied by the user. The units of the noise strength are given by the units of a_j and Δt . For example, a random walk in pulse phase (measured in pulse cycles with time measured in seconds) will have $m = 2$ and hence a noise strength $S = \langle P_{flattened} \rangle$ with the physical units of cycles²/s, whereas a random walk in pulse frequency ($m=4$) will have the physical units of cycles²/s³.

7. Power Spectrum Estimation of Simulated Red Noise Realizations with Uniform Sampling

We explored the practical estimation of power spectra of red PLN processes using simulated PLN time-series. This problem involved determining methods to generate PLN processes and then seeing if the predicted spectra and noise strength could be correctly recovered. Neither the generation of red PLN processes with non-even integer spectral indices nor high resolution estimation of their power spectra has been previously well developed, so sorting out the presence of possible systematic effects and attributing them to either the noise generation method or the spectral estimation method required extensive testing.

We implemented the time domain method of generating discrete red PLN realizations described in Appendix A. With this method a band limited white noise realization $\epsilon(t)$ is used as a basis upon which a power-law weight function acts to generate the red noise realization. The white noise is a zero mean process with a gaussian distribution of impulse amplitudes generated at times t_k with nonuniform time steps ($\Delta t = t_{k+1} - t_k$), where Δt is drawn from the exponential waiting time distribution of a Poisson process. The chosen step rate R_g and variance of the step amplitude distribution σ_ϵ^2 determine the noise strength $S = R_g \sigma_\epsilon^2$. The power-law weight function then acts upon the discrete white noise realization to produce a set of accumulated steps that can be sampled at an arbitrary set of times t_i that are independent of the times of the white noise impulses. For the case of a random walk, one will have a set of rectangular steps of varying amplitude and duration, whereas for $1/f^3$ noise, the individual steps will have a form $\propto t^{\frac{1}{2}}$. The appearance of the simulated noise realization for the same noise strength and power-law index varies appreciably depending on the sampling and step rates. For example, sampling at a rate greater than the white noise step rate R_g allows individual steps to be resolved. In figure 2 we portray a set of discrete red power law noise samples with resolved steps.

In figure 3 we show a set of red noise realizations generated from the same underlying white noise realization. As the power-spectrum becomes “redder” the time series takes on an increasingly smooth appearance that arises from the increasing dominance of the lowest frequency components. The right-hand set of panels shows the same noise realizations after

cubic polynomial detrending. A quasiperiodicity is apparent in the residuals in some cases that is a result of the polynomial detrending. Polynomial fits on shorter or longer timescales produce similar looking residuals and hence a “pseudoperiodicity” that scales with the length of the red noise time-series.

In the top panel of figure 4 we show an example of a $1/f^3$ noise realization that has been detrended by a cubic polynomial fit. All the time-series discussed in this section are uniformly sampled at a rate approximately twice the step rate and the results discussed apply strictly only for uniform sampling. In the middle panel we show the computed power spectrum (rough histogram) computed using a Hann window with $\alpha = 2$. Lying above this is a smoother histogram that shows the average power spectrum of 1024 similar noise realizations (shifted in power by 3 decades for display purposes). The simulations showed that the input power spectral slope and noise strength could be correctly recovered. The spectrum shows a clear turnover at low frequencies caused by the removal of low frequency power by the cubic polynomial detrending and this results in residuals that appear quasiperiodic. The average analysis frequency of the peak is purely related to the length of the data span fit. In the bottom panel we show the same power spectra after having been flattened as described in section 6 assuming a power-law index $m = 3$. We now see that the effect of the polynomial detrending is to *decrease* low frequency power in the flattened spectrum relative to higher frequencies. A high frequency upturn in the average spectrum is also present that is the result of aliased power from above the Nyquist frequency.

Examination of individual power spectra showed that cubic detrended realizations with a low number of zero-crossings (4-5) often displayed a slight excess of low frequency power with respect to the higher frequencies whereas those with higher numbers of zero-crossings tended to show a power deficit. This is an easily understood byproduct of the goodness of the cubic polynomial fit to the noise realization (i.e. better fits cause larger numbers of zero-crossings in the residuals). A second related effect is to produce a negative correlation of the mean squared value of the residuals with the number of zero-crossings, confirmed by simulations and is a general result for polynomial detrending of red noise. The degree of the polynomial fitting exhibited a weak positive correlation with the frequency of the power peak in the unflattened spectrum. This is expected since quartic and higher order polynomial detrending simply removes more low frequency power and hence shifts the power peak frequency to higher frequencies and results in a greater deficit of low frequency power in the flattened power spectrum.

Several effects of windowing and polynomial detrending are illustrated in figure 5 which displays averages of 1024 flattened power spectra for PLN realizations of unit strength with added white noise and a high frequency sinusoid. The power spectra were made using a Hann

window with $\alpha = 2$. First, the polynomial detrended power spectra show clearly the decrease in low frequency power relative to the power spectra produced from undetrended noise realizations. The relative power drop increases as the power-law index increases consistent with the fact that redder realizations are smoother and thus better fit by polynomials. Secondly, the undetrended power spectra show an excess of power at low frequencies which increases with the power-law index. This is probably a power leakage effect caused by leakage into the highest sidelobes of the power estimator which will be largest at low frequencies where most power is concentrated. Thirdly, another leakage effect is also readily apparent in figure 5 illustrated by the spectra of the undetrended realizations: namely that for power spectral estimation at higher frequencies power leaks into the entire low frequency side of the estimator and hence tends to get worse as the estimator’s nominal frequency increases. This effect eventually causes the spectral slope to change from the predicted power-law to a much lower value (≈ 2) when the increasing steepness of the power density spectrum causes the leaked power to exceed the rate of sidelobe fall-off of the power spectral estimator which for the Hann window with ($\alpha = 2$) is $\approx 1/f^6$. The polynomial detrending, by decreasing the lowest frequency power, which is the largest source of power leakage, decreases substantially both the local sidelobe leakage and the integrated leakage on the low frequency side of the estimator.

The high frequency area of figure 5 illustrates the dominance of the added white noise component at high frequencies as the red noise power level drops below that of the mean white noise power level. The “crossover” frequency is that power level where the mean red noise power level equals that of the white noise and occurs in this case near the frequency $f = 0.2$. The high frequency sinusoid added to the noise realizations clearly shows up as the narrow peak near $f = 0.1$. In general, the correct sinusoid frequency could be recovered from the flattened spectra with no more bias than in ordinary power spectral estimation.

We also tried other windowing functions such as the Hann window with $\alpha = 1$. This window has better frequency resolution but worse leakage protection than for $\alpha = 2$. Major leakage effects began to be noticeable for power-law indices for $m > 3.5$ for power spectra of nondetrended noise realizations and for $m > 4.4$ for detrended realizations. This is expected since the sidelobes fall-off as $\approx 1/f^4$. Other window functions such as the Hamming, Kaiser-Bessel or Bohman were examined as well but rejected due to their poor leakage protection. The Blackman-Harris window offered leakage protection comparable or better than the cosine windows in some frequency regimes but had noticeably worse frequency resolution due to the large width of the main lobe of the frequency response and so was rejected as well.

A second method of generating red PLN has been proposed by Timmer & König (1995) using a method that creates PLN realizations by generating the real and imaginary values of a

set of Fourier amplitudes and then weighting them by a power-law. The amplitudes are then Fourier transformed back into the time-domain. The use of a second method of generating PLN was useful in helping to differentiate effects caused by the spectral estimation technique versus those caused by the noise generation method. Direct comparison between the two noise generation methods was at first complicated by the lack of a proper normalization for the Timmer & König generated realizations. We determined a normalization for this method to generate noise with a predetermined noise strength consistent with that used for the time-domain method. See Appendix B for a more complete description.

The Timmer-König method generates a time-series from a discrete set of Fourier frequencies and is therefore missing power from frequencies not within the discrete set. Because of this, there is no power at frequencies higher than the Nyquist frequency, or lower than the lowest frequency $1/T$, where T is the total data timespan, as there would be in a more realistic segment of PLN. If the time-series is resampled at a higher rate, then a small aliasing effect can be observed in the power spectrum at the highest frequencies. Likewise, if the time-series is resampled at a lower rate then a deficit of power is apparent at the highest frequencies. If one uses the full time-series, then the endpoints and the derivatives of the lowest order frequency terms nearly match when the time series is cyclically repeated, which greatly reduces the power leakage problem. Thus we discarded the second half of the time-series to better represent true power-law noise. Without discarding the second half, flattened power-spectrum with the correct power and slope can be produced using only a rectangular window for power-law indices much greater than $m = 2$, e.g. upto at least $m = 5.5$! This is just a result of artificially constructing red noise only from harmonics that are exactly periodic on the analysis interval which causes all leaked power to fall exactly on the zero's of the *sinc* function frequency response.

Average power spectra similar to that of figure 5 were calculated for noise realizations generated by the Timmer-König method. These power spectra, similarly to those in figure 5, showed an excess in low frequency power for undetrended realizations and a subsequent drop in the power as a result of detrending. Major leakage effects set in at similar power-law indices. The only real differences were the lack of aliased high frequency power and different high frequency distortion effects for power-law indices $m \geq 5.5$ where the Hann window with $\alpha = 2$ ceases to provide adequate leakage protection.

8. Analysis of the 1982-1989 Crab radio timing residuals

8.1. Windowed Power Spectrum

We calculated a windowed power spectrum of the Jodrell Bank Crab timing residuals. The dense sampling and relative smoothness of the timing residual suggested that interpolation onto a uniform grid was possible without significant distortions. The timing residuals were first averaged on a one-day time scale, mainly to reduce the number of points in the densely sampled region after the 1986 glitch (see Lyne, Pritchard & Smith 1993 and figure 6, middle panel). The data were then interpolated onto a uniform grid using a cubic spline interpolation with $\Delta t = 1.346$ days. Two samples comparing the uniformly gridded phase residuals with the unprocessed phase residuals are shown in figure 7. Using the method described in section 6 a power spectrum was calculated using a Hann window with $\alpha = 1$. The uniformly binned time-series, windowed power spectrum and flattened power spectrum are displayed in figure 6. The power spectrum of the timing noise shows a power-law with a spectral index of $m = 3.09 \pm 0.05$. The flattened power spectrum shows a clear low frequency peak at a frequency $f \approx 0.0018$ cycles/day. In addition, the flattened power spectrum exhibits a decrease in low frequency power due to the removal of the polynomial trend and an upturn at high frequencies due to white noise in the pulse phase. A power spectrum was also calculated using a Hann window with $\alpha = 2$ (see bottom panel of figure 1) which provides better protection against red noise leakage but worse frequency resolution. Essentially the same power spectrum was produced but with worse resolution of the low frequency peak.

The power spectrum of the Crab timing residuals is consistent with the presence of a power-law noise component with a spectral index $m \approx 3$. The noise strength is given by the mean white noise level in the flattened spectrum. The averaged power in the flattened spectrum over the frequency range $0.003 - 0.1$ cycles/day is $(9.26 \pm 0.5) \times 10^{-7}$ cycles²/day². This implies a noise strength $S = (1.24 \pm 0.07) \times 10^{-16}$ cycles²/sec². The timing noise is consistent with a torque noise spectrum rising with analysis frequency as $\approx f$, implying *blue* torque noise, rather than white torque noise as found by Deeter (1981), Cordes (1980) and Groth (1975c). For the numerical 1st derivative of the uniformly binned time-series we repeated the power spectral analysis described above and found a spectral index $m = 1.12 \pm 0.05$ and a mean flattened noise power (assuming $m = 1$) of $(8.96 \pm 0.5) \times 10^{-7}$ Hz². Likewise, the numerical 2nd derivative had a spectral index $m = -0.86 \pm 0.05$ with a mean flattened noise power (assuming $m = -1$) of $(8.77 \pm 0.5) \times 10^{-7}$ (Hz/s)²day². Both these results are consistent with that for the pulse phase. A large peak in the power showed up clearly at the same analysis frequency in the flattened spectra for all three cases. The observed power spectrum of the pulse phase residuals is consistent with the presence of a power-law noise process, but we point out that this does not mean a power-law noise process

such as those described in appendix A is the correct form for the noise since there may be other noise processes that could produce similar power spectra.

The cubic spline interpolation onto a uniform grid could introduce some distortions in the computed power-spectrum, in spite of the relative smoothness of the Crab timing residuals. We checked the correctness of the analysis procedure described above using Monte Carlo simulations. A noise sample was generated by using the times of the Crab timing residuals after outliers had been removed. Using these sample times we generated a realization of $1/f^3$ power-law noise using the procedure described in Appendix A with a noise strength $S = 1.0 \times 10^{-6}$ cycles²/day² and a step rate $R_g = 0.7434$ day⁻¹. To this we added a white noise realization with a variance equal to the variance of the Crab timing measurement noise and a cosinusoid with parameters given in table 2. The realization was then fit by a quartic polynomial, averaged on a one day timescale and interpolated onto a uniformly gridded time-series using a cubic spline following the same procedure used in analysis of the actual Crab timing data. Power spectra of the resulting time-series were computed using Hann windows with $\alpha = 2$.

We generated a sample run of 512 simulated noise realizations, computed power spectra, and measured the power spectrum slope and noise power level in the flattened power spectrum over the frequency range 0.003 to 0.1 cycles/day. This frequency range avoided the low frequency power contribution of the cosinusoid and the high frequency white noise contribution. We found a mean PDS slope of -3.03 ± 0.15 and a mean power level of $(0.97 \pm 0.1) \times 10^{-6}$ cycles²/day², consistent with the input values. The peak frequency of the input cosinusoid was correctly recovered. A second similar run of 512 sample noise realizations without the low frequency cosinusoid was created and analyzed. A mean PDS slope of -3.03 ± 0.14 and a mean power level of $(0.98 \pm 0.1) \times 10^{-6}$ cycles²/day² was found. Any distortions due to aliasing would show up in the high frequency portion of the spectrum where the effects of white measurement noise tend to dominate and hence this is not a useful portion of the spectrum in any case. We therefore conclude that no significant distortions to the power spectra were introduced by the data analysis procedure described above.

8.2. Quasiperiodicity

The large low frequency peak in the Crab power spectrum appears to be a real feature and not simply a result of polynomial detrending of red noise. Detrended red noise should show a significant *decrease* in the low frequency power in the flattened spectrum relative to higher frequencies rather than an increase, as figure 4 demonstrates. The quartic polynomial removed from the Crab timing measurements will cause an even greater drop in low frequency

power in the flattened spectrum relative to that shown in figure 4 where cubic detrending was used. To investigate the significance of the power spectral peak we assumed the “white noise” in the flattened power spectrum followed a chi-square distribution. To check this assumption we made a histogram of the flattened power over the frequency range $f = 0.003 - 0.1$. The powers did indeed follow an exponential distribution. The peak at $f = 0.0018$ cycles/day has a probability of chance occurrence of less than 1×10^{-6} .

To determine whether the power spectrum peak was due to a periodic or quasiperiodic process we performed a sinusoidal fit to the Crab phase residuals in the low frequency region around the power spectrum peak. We represented the Crab phase residuals in the time domain with a model given by

$$\phi_{\text{model}}(t) = \phi_0 + \nu_0 \Delta t + \sum_{j=1}^4 \frac{d^j \nu}{dt^j} \frac{\Delta t^{j+1}}{(j+1)!} + A \cos(2\pi f \Delta t) + B \sin(2\pi f \Delta t) \quad (14)$$

where f is the sinusoid frequency and $\Delta t = t - t_0$ where $t_0 = \text{TJD } 6390$ is an epoch. This model was fit to the data by doing a modified-Marquardt fit to the linear terms for each sinusoid frequency in a grid. For each frequency, a fit statistic was computed, given by

$$\Delta\chi^2 = \chi_{\text{poly}}^2 - \sum_{i=1}^N \frac{|\phi_i - \phi_{\text{model}}(t_i)|^2}{\sigma_i^2} \quad (15)$$

where χ_{poly}^2 is computed for a fourth order polynomial model (no sinusoid) and ϕ_i are the Crab phase residuals with errors σ_i .

First sinusoid frequencies in a wide range (0.5 to 4.0 cycles per 1000 days) were searched. This search found a peak in $\Delta\chi^2$ at $f \approx 1.76$ cycles/kday (equivalent to a period of 568 days) and a gradual increase in $\Delta\chi^2$ as the frequency decreased below about 1 cycle/kday. Next a narrower search (1.26-2.26 cycles/kday), centered on the peak was performed to refine the fit. The best fit with frequency was $f \approx 1.762$ cycles/kday (or $P \approx 567.5$ days) with a sinusoid amplitude $(A^2 + B^2)^{1/2} \approx 0.26$ cycles.

To estimate the probability of finding a peak at this frequency by chance and to place errors on the parameters, two sets of Monte-Carlo simulations were performed. In the first set of simulations, the model above was fitted to 10000 red-noise realizations and the best-fit frequencies were retained. The red noise consisted of simulated power-law noise using the time-domain method described in Appendix A with a power-law index $m = 3$ and noise strength $S = 1.0 \times 10^{-6}$ cycles²/day², equivalent to that found for the Crab pulsar. The same data sampling as the Jodrell Bank data was used. A distribution of the best-fit frequencies was obtained that had a maximum near the frequency 0.88 cycles/kday and a broad low frequency tail. In the second set of simulations a sinusoid with the parameters in

Table 2 was included. The resulting distribution of best-fit frequencies was tightly clustered around a maximum frequency of 1.76 cycles/kday. For the case with no sinusoid present, a total of 69 trials fell in the frequency range 1.736 to 1.790 cycles/kday, the full width of the distribution of best-fit frequencies with the sinusoid present, suggesting a probability of chance occurrence of 6.9×10^{-3} . However, the largest sinusoid amplitude measured in this frequency range was ~ 0.11 , about 2.3 times smaller than the amplitude measured in the actual Crab data. Also, the largest $\Delta\chi^2 = 6.9 \times 10^7$, was about 5.4 times smaller than that measured in the data. These additional factors suggest that the probability that this peak is due to some systematic effect is smaller than 6.9×10^{-3} .

The errors on the fitted sinusoid parameters were estimated from the set of 10000 fits to the simulated red-noise realizations with a sinusoid present. The obtained parameter distributions were approximately gaussian and parameter errors were determined from gaussian fits to the distributions for the sinusoid frequency, cosine amplitude, and sine amplitude respectively. The parameters and their errors were also converted to their equivalent representation for a single cosine and phase⁴. Table 2 lists the best fit parameters along with their estimated errors.

The low frequency oscillation in the 1982-1989 Crab phase residuals appears to be nearly periodic. This is suggested by the fact that when the power spectrum is recomputed after removal of the best fit sinusoid, essentially all excess power in the frequency range of the peak is removed. However, since less than five cycles are present in the stretch of Jodrell Bank data analysed here, and longer data stretches are interrupted by the occurrence of data gaps or large glitches, the long term coherence of the low frequency oscillation is not known.

8.3. The 1986 Glitch

We investigated the effect of the 1986 glitch (Lyne, Pritchard & Smith 1993) on the power spectrum. We tried simply deleting the glitch from the phase residuals or fitting a function to the glitch in order to smooth over the glitch interval. We excised the glitch over the interval TJD 6664.4 to TJD 6746.0. When this was done the spline interpolation filled in the empty gap with a linear segment. The computed window power spectrum (using a Hann window with $\alpha = 1$) exhibited a slight change in slope from -3.09 ± 0.05 to -3.12 ± 0.06 over the analysis frequency range 0.003 – 0.1 cycles/day. The mean power in flattened power spectrum dropped significantly from a level of $9.26(\pm 0.49) \times 10^{-7}$ to $5.3(\pm 0.3) \times 10^{-7}$ cycles²/day³. The power at highest and lowest frequency portions of the PDS was unaffected.

⁴ $\phi_{QP}(t - t_0) = A_0 \cos(2\pi(t - t_0)/P - \Phi_0)$ where the single cosine amplitude is given by $A_0 = (A^2 + B^2)^{\frac{1}{2}}$.

In contrast, when random sections of data of equal duration were removed, there was almost no effect on either the power spectral slope or the mean power level in the flattened spectrum.

The second method used a fit to the glitch involving several steps. First the phase residuals from the preglitch interval one month prior to the glitch were fit with a linear function. This was extrapolated into the glitch interval and subtracted. A glitch function of the form:

$$\phi(t) = 86400\nu_1\tau_1(\exp(-t/\tau_1) - 1)$$

where $\nu_1 = 1.73 \times 10^{-7} \text{ Hz}$ and $\tau_1 = 6.3 \text{ days}$ was then subtracted. A rising phase residual was left that was fitted with a quadratic polynomial and subtracted as well, leaving flat phase residuals with no systematic trends. When this set of functions was removed from the phase residuals, the phase residuals exhibited a linear trend in this interval. The result on the computed power spectrum was essentially the same as in the case of the simple excising above: a slope of -3.11 ± 0.06 and mean power level in the flattened power spectrum of $5.6(\pm 0.3) \times 10^{-7} \text{ cycles}^2/\text{day}^3$ over the analysis frequency range $0.003 - 0.1 \text{ cycles/day}$.

Either method of treating the glitch showed that a considerable amount of power resulted from the glitch but without any change in the power-law slope. Thus the noise strength estimated for the timing noise may be too high by a factor of two.

9. Deeter Polynomial Power Spectral Estimation

We computed power spectra of red PLN processes and of the Crab timing residuals using the Deeter polynomial method and compared them to power spectra computed using windowing methods. We did this as a cross check on both power spectral estimation procedures and as a direct comparison with previously reported Crab timing analysis. The Deeter polynomial method of power spectrum estimation is directly applicable in the case of nonuniformly sampled data, unlike windowing methods, but produces power spectra of low spectral resolution. After comparing a number of procedures for estimating the power spectrum of a red-noise process, Deeter (1984) concluded that a technique based upon sampling with orthonormal polynomials on a hierarchy of time scales produces a good power spectrum with modest frequency resolution. Specifically, Deeter (1984) proposed constructing power spectra with approximately octave frequency resolution by iteratively partitioning a data set into increasing numbers of shorter segments. For each segment, an amplitude is obtained by constructing a set of polynomials that are orthonormal on the segment and using the highest order polynomial from the set to “sample” the data by forming the sum of the product of

the time series with the highest order polynomial, i.e.,

$$a = \sum_k \phi_k h_k, \quad (16)$$

where ϕ_k is the measured phase and $h_k = p(t_k)/\sigma_k^2$, where $p(t_k)$ is the (highest order orthonormal) polynomial evaluated at time t_k , the time of the k th phase, and σ_k is the measurement uncertainty of the k th phase. The square of the amplitude, a , is an estimate of the power in the segment. For each partitioning, the average of the powers in the segments is an estimate of the power in the time series, at the time scale of the segments. By repeating the procedure for each partitioning, and by converting time scales to frequencies, a power spectrum of the white noise underlying the red noise is constructed.

For a given set of times and weights, there is a unique set of orthonormal polynomials. For example, for the continuous interval $[-1, 1]$ with uniform weight, they are the Legendre polynomials. It is not difficult to show that the amplitude obtained by sampling with the highest order polynomial in a set of orthonormal polynomials is equal to the coefficient of the highest order term in a polynomial fit to the data with the same order, l , as the highest order orthonormal polynomial. We chose to fit, rather than sample, and refer to this technique as the *Deeter polynomial power spectrum estimation method* or more simply as the *Deeter polynomial method*. We have applied this technique in the case of accretion-powered pulsars in Bildsten et al. 1997.

As a direct comparison of the Deeter polynomial method to the windowing method we applied each method to the same simulated red PLN time-series. In figure 8 we show the average power spectra computed using each technique for the same 32 uniformly sampled noise realizations. The noise is $1/f^3$ PLN generated using the time domain method and detrended by a cubic polynomial fit. The spectra have been flattened for the case of a $1/f^3$ power-law, which involves dividing the Deeter polynomial power spectrum by a factor $2\pi f$. Sinusoids have also been added in four of the five spectra displayed. In general, when pure red PLN was present the two techniques gave consistent results as can be seen in the third spectra from the top, although the normalization of the Deeter polynomial method has to be adjusted somewhat depending on the assumed noise present. When strong discrete features were present in the power spectra, considerable power leakage occurred due to the low spectral resolution of the Deeter polynomial estimators and hence distorted the power spectra. In general, the presence of significant discrete features can cause considerable ambiguity in the interpretation of the Deeter polynomial power spectra.

A Deeter polynomial power spectra was computed for the Jodrell Bank Crab timing residuals and is displayed in figure 1. The Crab timing residuals used in the computation are shown in the top panel of figure 1 and were subjected only to the dispersion measure

corrections and removal of outliers described in section 3. No averaging or interpolation was done. The computed power spectrum for the pulse frequency rate of the phases is shown in the middle panel of figure 1. The power contributed by measurement noise is shown by the triangles and has not been subtracted off from the total power shown by the solid circles, which is the convention used in this paper. If the timing residuals consisted of pure $1/f^4$ noise in pulse phase as claimed by several previous analysis the power spectrum would be flat. A distinct rise with frequency can be observed at frequencies greater than $\log f = -2.5$, although the large amount of power at $\log f = -2.9$ might cause one to argue that the spectrum is actually flat. When the spectrum is divided by $2\pi f$ (bottom panel of figure 1), which will produce a flat spectrum if $1/f^3$ noise is present, a flat spectrum is indeed produced except for a peak near $\log f = -2.9$. For comparison, we also plot the power spectrum (histogram) computed using a Hann window with $\alpha = 2$ for the uniformly sampled time series displayed in the top panel of figure 6. The power spectra are similar except for a deficit in power in the Deeter polynomial spectrum near $\log f = -2.6$, relative to the windowed spectrum.

Since past analysis of the Princeton optical timing observations have concluded that the timing noise in the Crab pulse phase is $1/f^4$ noise (Groth 1975c, Cordes 1980, Deeter 1981) rather than the $1/f^3$ noise found above, we also investigated this data set to see why this was the case. In figure 9b we show a Deeter polynomial power spectrum calculated using the same Princeton optical data set used by Deeter (1981), which is displayed in figure 9a. The power spectrum calculated by Deeter can be found as figure 8 in Alpar, Nandkumar & Pines (1986). The spectrum is calculated for the pulse frequency derivative and hence will be flat for pure $1/f^4$ noise in pulse phase. The spectrum in our figure 9 is relatively flat but shows an increase in power at low frequencies. When flattened under the assumption of $1/f^3$ noise we see that the spectrum is again relatively flat with a relatively greater excess of power at low frequencies very similar to that found for the Jodrell Bank data set. However, as the Princeton data set is somewhat shorter than the Jodrell Bank data set, the excess low frequency power appears more as a curvature in the spectrum rather than a discrete peak. We therefore conclude that the spectrum is consistent with either an interpretation as $1/f^4$ noise in pulse phase or as $1/f^3$ in pulse phase combined with a low frequency periodic or quasiperiodic process. In the absence of any motivation to assume that a large amplitude low frequency quasiperiodic process was present, clearly it would be more natural to assume that only $1/f^4$ noise in pulse phase was present, although Groth (1975c) did speculate about the presence of a small contribution from $1/f^2$ noise in pulse phase.

A cubic spline interpolation of the Princeton optical timing residuals onto a uniform time series was made and a windowed power spectrum computed for the sake of completeness. The interpolated time series is shown in figure 9a offset below the actual timing measurements.

When a Hann windowed power spectrum with $\alpha = 2$ was computed, a slope of -3.2 ± 0.08 between the analysis frequency range of $0.003 - 0.1$ cycles/day. The power spectrum flattened under the assumption of $1/f^3$ noise is shown as the histogram in figure 9c. For the same frequency range, a mean noise level of $(4.9 \pm 0.37) \times 10^{-7}$ cycles²/day² is measured, about half that for the Jodrell Bank phase residuals. The windowed power spectrum is remarkably similar to the Deeter polynomial power spectrum and shows a similar large low frequency bump. The interpolated time series is clearly in error from the true time series since the gaps tend to be filled with linear segments. However, neither method of power spectrum computation has information within the gaps and the lowest order polynomials in the Deeter polynomial power spectrum also involve fitting across gaps and hence also involve a form of interpolation. Since the data are likely to be relatively smooth at the lowest analysis frequencies, these interpolations may not introduce any major distortions to the power spectrum.

10. Discussion

The timing noise in the Crab pulsar has been claimed to be either a white torque noise process or a quasiperiodic process. As a result of the analysis presented here, the timing noise or rotational irregularities in the pulse phase of the Crab pulsar appear to be composed of two components: a noise process with a $1/f^3$ power spectrum and a periodic or nearly periodic process with a period of approximately 568 ± 10 days. A noise process with a $1/f^3$ power spectrum in pulse phase becomes a process with a spectrum rising as f in the pulse frequency derivative, so the timing noise in the pulse frequency derivative (or torque for the case of a constant moment of inertia for the neutron star) has a *blue* power spectrum.

The argument for $1/f^3$ noise rests on the windowed power spectrum of the timing residuals obtained from the Jodrell Bank radio observations over the period 1982 - 1989. The windowed method of power spectrum computation was thoroughly checked with simulated noise data and appears to be a quite reliable method in this situation of relatively smooth residuals and high density sampling. The result is reinforced by a Deeter polynomial power spectrum of this same data which yielded a consistent result. A Deeter polynomial power spectral analysis of the Princeton Crab optical timing data previously analyzed by several investigators (Groth 1975b,c, Cordes 1980 and Deeter 1981), showed that this shorter and more sparsely sampled data set was consistent with either a pure $1/f^4$ noise process or a $1/f^3$ noise process with a large excess of low frequency power, thus explaining why previous analyses chose the simpler interpretation of pure $1/f^4$ noise.

Many theoretical studies have proposed models for the timing noise observed in radio

pulsars involving internal or external torques acting on the neutron star crust. A good summary and references can be found in D’Alessandro (1997). Many of these models have been developed to the point that they make predictions about the form of the power spectrum of the torque noise. In the vortex creep model (see Alpar, Nandkumar & Pines (1986)), several predicted torque power spectra are proposed that are flat with a transition over some characteristic frequency range to another flat region or are flat at high frequencies but transition over to a $1/f^2$ power-law at low frequencies. None of these models match the spectrum observed for the Crab pulsar. In the internal torque noise model of Jones (1990), the predicted power for the torque noise is a superposition of red and white components and also does not match the spectrum observed for the Crab pulsar. The external torque noise model of Cheng (1987) predicts either a blue or white spectrum for the torque noise but the blue component is a f^2 power-law rather than f . There does not seem to be any current model that predicts a blue pulse frequency derivative noise power spectrum rising as f .

An excess of power in both the windowed and Deeter polynomial power spectrum is apparent at low frequencies indicating the additional presence of a strong quasiperiodic or periodic process. A known property of red power-law noise processes (or any noise process with a red spectrum) is that polynomial detrending will produce quasiperiodic residuals that are purely an artifact of the detrending. These quasiperiodicities have occasionally been considered real by investigators unfamiliar with this property of red noise. However, we show the quasiperiodicity present in Jodrell Bank Crab timing residuals is real. This is indicated by the presence of a peak in the low frequency power in the flattened windowed power spectrum rather than the deficit of power that would occur if the quasiperiodicity was spurious. The sharpness of the low frequency peak also argues against this being the result of a step in the power spectrum coupled with low frequency power removal caused by detrending although we did not investigate this possibility in depth.

The coherence of the low frequency quasiperiodic oscillation was investigated by fitting a sinusoid + quartic polynomial to the timing residuals using a linear least squares technique. The removal of this sinusoid also removed most of the excess power in the peak in the flattened windowed power spectrum (as well as in the Deeter polynomial power spectrum) indicating that the process is more nearly periodic than quasiperiodic. Another indication of the near periodicity is the comparison of the fitted sine to the 1st derivative of the Crab pulse phase timing residuals which revealed four clear oscillations after TJD 5500 (see figure 7). Before TJD 5400 a possible phase shift and amplitude change may have occurred showing that the oscillation process may be incoherent on time scales longer than 2000 days. Inspection of the 1st derivative plot also revealed a possible small glitch occurring near TJD 5243 based on the occurrence of a large amplitude spike that resembles the large amplitude spike caused by the known small glitch at TJD 6664. However, the data sampling around this second

possible small glitch is too sparse to make this conclusive (see figure 7). The occurrence of the glitch(s) does not seem to be related to the phase change in the long term oscillation since the phase was not clearly affected by the glitch at TJD 6664.

The possible origin of the periodic or nearly periodic process has been discussed before by Lyne, Pritchard & Smith (1988). Explanations include oscillations of the superfluid vortex lattice (Tkachenko oscillations), free precession of the neutron star or the presence of an orbiting companion. The 568 day period is roughly comparable to the 1000 day timescales observed in a few radio pulsars that may be exhibiting free precession (e.g Stairs, Lyne & Shemar, 2000). If the neutron star is freely precessing then long period pulse shape changes should be observable as well but no significant detections of this effect have been reported to date. If an orbiting companion is causing the observed rotation oscillations we can derive limits on orbital parameters. Assuming a binary companion with a circular orbit, we can determine an $a_x \sin i = (8.65 \pm 1.0) \times 10^{-3}$ lt – sec from the cosine amplitude given in table 2 and a mass function

$$f(M) \equiv \frac{4\pi(a_x \sin i)^3}{GP_{orb}^2} = \frac{(M_c \sin i)^3}{(M_x + M_c)^2} = (6.8 \pm 2.4) \times 10^{-16} M_\odot. \quad (17)$$

If we assume a Crab pulsar mass of $M_x = 1.4 M_\odot$ and a value of $\sin i = 1$ we can determine a lower limit on the companion mass of $M_c \geq 3.2 M_\oplus$ and a projected orbital radius $a_c \sin i = 750 \pm 93$ lt-sec or 1.50 astronomical units. The presence of a planet around the Crab pulsar is an exciting possibility but requires confirmation by detection of the coherent oscillation on longer timescales before this could be considered the definitive explanation. Caution must be emphasized here as planets have often been claimed to explain the polynomial-like timing residuals of pulsars but have later failed to be confirmed (e.g. Konacki et al. 1999), although it must also be emphasized that the longterm periodicity or quasiperiodicity here detected in the Crab pulsar is a real timing component and not merely an artifact of fitting red noise.

Lastly, we speculate on a possible external origin for most of the power in the $1/f^3$ timing noise component of the pulse phase. The mechanism causing the timing noise would have to have an amplitude that increases with analysis frequency, a characteristic shared by the gravitational perturbations caused by a body in a Keplerian orbit on its companion. Given that a planet may be in orbit around the Crab pulsar could there also be a disk of smaller bodies or planetesimals as well? The collective gravitational perturbations from a “disk” of planetesimals acting on the neutron star will be a source of timing noise. A planetesimal of mass m in a circular orbit with radius r around a neutron star with a mass $M_x = 1.4 M_\odot$ will have a Keplerian orbital frequency (in cycles/day) given by:

$$\nu_{orb} = 36.17 r^{-\frac{3}{2}} \quad (18)$$

where r is given in lt – sec. The amplitude of the sinusoidal timing signature (in seconds) will be given by $\tau = (m/M_x)(r/c)$ where c is the speed of light. Now if we assume that the average planetesimal mass scales with orbital radius, as might be the case if the planetesimals condensed out of a uniform density disk, then $m = kr$. Substituting into the relationship for τ and solving for r in terms of ν_{orb} we get:

$$\tau = 119.7(k/M_x)(\nu_{orb})^{-\frac{4}{3}}. \quad (19)$$

The superposition of timing signatures from many planetesimals over a wide range of orbits will result in a power spectrum of the pulse phase with a slope of $-8/3$ - very close to the observed slope of -3 .

We tested this idea using a Monte Carlo simulation by simulating a set of 128 planetesimals with random initial orbital phases and a range of orbital frequencies from 0.001 – 1 cycles/day distributed uniformly in the logarithm. We fixed the constant k by choosing a planetesimal mass at $r = 750$ lt – sec. For mass distributions with $m = kr$, the power spectral slopes tended to be near -3.7 , too small to fit the Crab pulsar. For a planetesimal mass distribution with $m = kr^{\frac{1}{2}}$ and a planetesimal mass of $1.62M_{\oplus}$ at $r = 750$ lt – sec, the average slope of the power spectrum was near -3 over the frequency range 0.003–0.1 cycles/day, with an average noise level in the flattened power spectrum of 1×10^{-6} cycles²/day² - matching that observed for the Crab pulsar. To fully model the Crab timing residuals the planetesimal at $r = 750$ lt – sec must be replaced with a planet of mass $M \geq 3.2M_{\oplus}$. Whether such a planetesimal mass distribution and set of orbits is reasonable and physical is a question beyond the scope of this paper.

The power spectrum of the timing caused by a planetesimal disk can be calculated analytically as well. The phase signature of the the disk of planetesimals is

$$\Delta\phi(t) = \sum_k x_k \cos(2\phi\nu_k t + \psi_k) \quad (20)$$

where the sum is over plantesimals k , and x_k , ν_k , and ψ_k are the phase amplitude, orbital frequency, and orbital phase respectively of plantesimal k . The phase amplitude x_k is given by

$$x_k = \nu_o r_k \sin i m_k M^{-1} c^{-1} \quad (21)$$

with r_k the orbital radius and m_k the mass of plantesimal k , i is the inclination of the disk, and M the total system mass. The orbital radius is related to the orbital frequency by

$$r(\nu) = (GM)^{1/3} (2\pi\nu)^{-\frac{2}{3}}. \quad (22)$$

If we assume the orbital phases ψ_k are independent then the autocorrelation function of $\Delta\phi$ is

$$A_{\Delta\phi}(\tau) = \frac{1}{2} < \sum_k x_k^2 \cos(2\pi\nu_k\tau) > . \quad (23)$$

If the density of planetesimals per unit radius r is given by $D(r)$ and the planetesimal mass distribution at radius r is given by $P(m|r)$ then the autocorrelation function is expected to be

$$\begin{aligned} A_{\Delta\phi}(\tau) &= \frac{1}{2} \int D(r)P(m|r)(\nu_o r \sin i m M^{-1} c^{-1})^2 \cos(2\pi\nu(r)) dm dr \\ &= \int \mathcal{S}(\nu) \cos(2\pi\nu\tau) d\nu \end{aligned} \quad (24)$$

where we have changed integration variables using equation 22, and

$$\mathcal{S}(\nu) = \frac{1}{3} \pi \nu_o^2 \sin^2 i G M^{-1} c^{-2} (2\pi\nu)^{-3} D(r(\nu)) m^2(r(\nu)) \quad (25)$$

with

$$m^2(r) = \int P(m|r) dm \quad (26)$$

being the mean square planetesimal mass are radius r .

$\mathcal{S}(\nu)$ is the power spectrum of the phase component $\Delta\phi$. If $D(r)m^2(r)$ is a powerlaw in r with index α , then $\mathcal{S}(\nu)$ will be a powerlaw in ν with index $-(3 + 2\alpha/3)$. The measured ν^{-3} power spectra implies that $\alpha \approx 0$. From the strength of the power spectrum we find that

$$D(r)m^2(r) \approx 2.1 \sin^{-2} i M_{\oplus}^2 \text{Au}^{-1} \quad (27)$$

in the radius range $0.13 < r < 1.3 \text{Au}$.

Remnant disks of heavy elements formed by fallback material from the supernova explosion that gave birth to the neutron star have been proposed as explanations for phenomena observed in radio pulsars and anomalous X-ray pulsars (e.g. Lin et al. 1991, Alpar 2001). A potential planet or planets around the Crab pulsar would probably have to come from preexisting planets that survived the supernova rather than being assembled from planetesimals given the short time (< 1000 years) since the Crab supernova occurred although the effect of a pulsar wind on a dust disk might significantly speed up the formation of planetesimals by concentrating the orbiting dust into preplanetesimal pockets. In addition to the cases of a pure fallback disk or surviving planets one can also envision mixed scenarios in which supernova surviving planets interact with a supernova fallback disk or a planetesimal disk forms through the collision of a planet with another body.

The presence of a planetesimal disk causing the timing noise in the Crab pulsar and possibly in other radio pulsars with significant timing noise would have some wider implications if validated. The fall back scenarios proposed for anomalous X-ray pulsars (AXP's, for a review see Mereghetti et al. 2002) have tended to consider only gaseous accretion disks. Large gaseous disks could supply the spin-down torque observed in these systems and supply accreting material to produce the persistent X-ray emission, but cannot explain the recently observed X-ray bursts (Gavriil et al. 2002) that support the idea that the related X-ray burst emitting soft gamma repeaters and anomalous X-ray pulsars form a single class of objects. In addition, searches for optical counterparts do not support the presence of large gaseous disks in such systems (e.g. Hulleman et al. 2000). Thus, by default, the alternative magnetar theory has gained much recent support. In contrast to a large gaseous disk, a toroidal swarm of planetesimals would be more easily hidden from view and could supply material in the form of gas for steady accretion as planetesimals are tidally broken up near the neutron star and form an inner gaseous ring or as dust formed further out, perhaps through planetesimal intradisk collisions, migrates inwards under the Poynting-Robertson effect or from drag in a pulsar wind. Planetesimals beyond the tidal radius could also supply material for series of occasional X-ray bursts if a planetesimal gets fragmented as a result of an intradisk collision and the low angular momentum pieces gradually rain down onto the neutron star in an event analogous to a meteor storm. Alternatively, a planetesimal could have its orbit disrupted into a comet-like path by a close encounter with one of the largest disk members and eventually collide with the neutron star causing a giant outburst. Series of smaller outbursts could also occur before, during and after the main body collides with the neutron star, if the planetesimal is broken up by a close orbital pass by the neutron star prior to or during the orbital pass of the primary collision. Either scenario would cause occasional bursts of X-rays to be emitted by the neutron star. Thus a planetesimal disk has the potential of explaining both the persistent X-ray emission observed, the slowing down of the neutron star spin, sets of occasional small and giant X-ray bursts and the observed lack of a large gaseous accretion disk. In addition, the observations of transient infrared emission associated with several AXP's after X-ray bursts have been detected (e.g. Israel et al. 2002) could be related to the formation of these temporary orbiting dust or debris clouds.

Chandra X-ray observations reveal an equatorial torus of material around the Crab pulsar (Weisskopf et al. 2000) that might be supplied by ablation and/or tidal disruption of planetesimals from an inner disk. The radius of the observed torus is on the order of 0.4 parsecs, while the disk considered here is within 1.5 astronomical units of the pulsar - far too small to be imaged directly.

The fast rotation of the Crab pulsar would place it in a propellor phase in which the outward flow of momentum from the pulsar exceeds the gravitational energy of the incoming

material. This would result in a particle outflow and possibly cause the observed jet from the Crab pulsar. The rate of spindown torque on the neutron star would also be increased relative to the vacuum case, lowering the braking index from the canonical value of 3 for the emission of pure magnetic dipole radiation. However, to observe gravitational effects on the neutron star it is not necessary that the planetesimals or any derivative dust must be interacting directly with the pulsar magnetosphere at the present time.

A group of planetesimals with a total mass of a few dozen Earth masses could plausibly cause the timing noise in the Crab pulsar and would have a mass similar to that required of the postulated “fallback” disks of the anomalous X-ray pulsars and soft gamma repeaters. If the scenario outlined here is correct, the Crab pulsar could eventually evolve into an anomalous X-ray pulsar or soft gamma repeater when the neutron star rotation slows to the point that accretion becomes possible. If other pulsars have planetesimal disks, then the power spectral indices of their timing noise might be expected to have a fairly wide range, caused by differing disk mass distributions and one might observe real quasiperiodicities as well in their timing noise due to the largest bodies orbiting the neutron star.

We thank Andrew Lyne for kindly providing the Jodrell Bank Crab timing data and Robert Pritchard for help in the initial analysis. We also thank Paul Boynton for useful discussions and for help in the early stages of this project.

A. Generation of Red Power-Law Noise Using Power-Law Weighting of White Noise

Power-law noise (PLN) processes with negative even integer spectral indices can be produced by the repeated integration of a white noise process $\epsilon(t)$. For example, a random walk, with a $1/f^2$ power spectrum, is defined as:

$$r_2(t) = \int_{-\infty}^t \epsilon(t') dt'. \quad (\text{A1})$$

We consider $\epsilon(t)$ to be a zero-mean white noise process defined for all t with an autocovariance function $\langle \epsilon(t)\epsilon(t+\tau) \rangle = \sigma_\epsilon^2 \delta(\tau)$, where $\delta(t)$ is the Dirac delta-function. An equivalent way of defining $r_2(t)$ is as the convolution of white noise with the unit step function, $H(t)$:

$$r_2(t) = \epsilon(t) * H(t) = \int_{-\infty}^{+\infty} \epsilon(t') H(t-t') dt' = \int_{-\infty}^t \epsilon(t') dt' \quad (\text{A2})$$

where $H(t)$ is the standard Heaviside step function defined as: $H(t) = 1$; $t \geq 0$ and $H(t) = 0$; $t < 0$. Now a $1/f^4$ noise process, produced by the integration of $r_2(t)$, can be

made instead by convolving $H(t)$ with $r_2(t)$, but this is equivalent to first convolving $H(t)$ with itself and then convolving the resulting function with $\epsilon(t)$:

$$H(t) * (H(t) * \epsilon(t)) = (H(t) * H(t)) * \epsilon(t). \quad (\text{A3})$$

The self convolution of $H(t)$ results in a ramp function: $tH(t)$. Therefore $r_4(t)$ can be generated directly as the convolution of $tH(t)$ with white noise:

$$r_4(t) = (tH(t)) * \epsilon(t) = \int_{-\infty}^t (t - t') \epsilon(t') dt'. \quad (\text{A4})$$

The convolution of $\epsilon(t)$ with $t^2 H(t)$ will generate $1/f^6$ noise. In general, even-integer red PLN can be generated directly from white noise as:

$$r_m(t) = \frac{1}{k!} \int_{-\infty}^t (t - t')^k \epsilon(t') dt' \quad (\text{A5})$$

where the power-law spectral index $m = 2(k + 1)$ and $m = 2, 4, 6 \dots$ without the need for repeated integration. Note that a normalization factor of $\frac{1}{k!}$ has been added. Given this formulation for $r_m(t)$, there is no *a priori* reason to restrict k to positive integer values and we consider the generalization of this formulation to noninteger k .

The noise process described in equation (A5) is a member of the class of general linear noise processes (see e.g. Priestley, 1981, p. 177) with the form:

$$r(t) = \int_{-\infty}^t w(t - t') \epsilon(t') dt' \quad (\text{A6})$$

in which a weight function of the form $w(t)H(t)$ is convolved with white noise. This form has many easily analyzable properties. For example, the ensemble averaged PDS can be calculated from the multiplication of the Fourier transform of $w(t)H(t)$ with that of $\epsilon(t)$. Thus $r(t)$ can be described in terms of the “noise strength” S and the weight function of the form $w(t)H(t)$ in the time domain or the spectral shape of the PDS in the frequency domain. In the case of discrete white noise, the weight function can be viewed simply as a “step” so that the noise process can be viewed as an accumulation of random steps with a similar form. For example, a random walk is an accumulation of the step functions $H(t)$, occurring with random amplitudes and at random times. If the duration of the step is finite the noise process will be asymptotically stationary since two values of the noise process separated by a sufficiently large time interval will be uncorrelated. In the well known case of “shot noise” the step is a decaying exponential, so values of the noise process are correlated on short timescales and approach an uncorrelated state on long timescales. This is reflected in the PDS of shot noise, which is flat at low frequencies but turns over to a power-law at high

frequencies. For red power-law noise proceses a correlation exists between a given value and all past values of the time-series, but the statistical properties are the same at any time t so the process is stationary.

Let us look at a specific power-law weight function before moving onto the more general case. If $k = -\frac{1}{2}$ so $w(t)H(t) = \frac{1}{\sqrt{\pi}}t^{-1/2}H(t)$, where the generalized definition of $k! = \Gamma(1+k)$ has been used, then the Fourier transform will be given by:

$$F(f) = \frac{1}{\sqrt{\pi}} \int_0^{+\infty} t^{-1/2} (\cos(2\pi ft) - i \sin(2\pi ft)) dt. \quad (\text{A7})$$

The resulting Fourier transform is:

$$F(f) = (1 - i) \left(\frac{1}{2\sqrt{\pi f}} \right) \quad (\text{A8})$$

with a power density spectrum of the form:

$$P(f) = F(f)F^*(f) = \frac{1}{2\pi f}. \quad (\text{A9})$$

Multiplication by the PDS of $\epsilon(t)$ creates the well known $1/f$ noise power spectrum.

The general power-law problem involves solving Fourier transforms of the weight function $W(t) = \frac{t^k}{k!}H(t)$:

$$F(f) = \frac{1}{k!} \int_0^{+\infty} t^k (\cos(2\pi ft) - i \sin(2\pi ft)) dt. \quad (\text{A10})$$

The Fourier integral will not in general converge since the time-series has infinite “energy” but we can solve directly for a few special cases. For example, if $-1 < k < 0$ the integrals have the solutions:

$$F(f) = \frac{\pi}{2\Gamma(|k|)\Gamma(1+k)} \left(\frac{1}{\sin(\frac{|k|\pi}{2})} + \frac{i}{\cos(\frac{|k|\pi}{2})} \right) (2\pi f)^{-(k+1)} \quad (\text{A11})$$

and the power spectrum is given by:

$$P(f) = \frac{\pi^2}{4(\Gamma(|k|)\Gamma(1+k))^2} \left(\frac{1}{\sin(\frac{|k|\pi}{2})^2 \cos(\frac{|k|\pi}{2})^2} \right) (2\pi f)^{-2(k+1)}. \quad (\text{A12})$$

When $k = -\frac{1}{2}$ then (A11) and (A12) reduce to the previous results (A8) and (A9) for $1/f$ noise.

Although the Fourier transform can't be solved directly it can be solved as a limit. If we add an exponential cutoff we get an integral of the form:

$$F(f) = \frac{1}{k!} \int_0^{+\infty} e^{-\frac{t}{\lambda}} t^k (\cos(2\pi f t) - i \sin(2\pi f t)) dt \quad (\text{A13})$$

The integral solutions to the cosine and sine portions of the integral can be found in integral tables and are, respectively:

$$\frac{1}{k!} \int_0^{+\infty} e^{-\frac{t}{\lambda}} t^k \cos(2\pi f t) dt = \frac{[(\frac{1}{\lambda} - i2\pi f)^{k+1} + (\frac{1}{\lambda} + i2\pi f)^{k+1}]}{2(\frac{1}{\lambda^2} + (2\pi f)^2)^{k+1}} \quad (\text{A14})$$

and

$$\frac{1}{k!} \int_0^{+\infty} e^{-\frac{t}{\lambda}} t^k \sin(2\pi f t) dt = \frac{[(\frac{1}{\lambda} + i2\pi f)^{k+1} - (\frac{1}{\lambda} - i2\pi f)^{k+1}]}{2i(\frac{1}{\lambda^2} + (2\pi f)^2)^{k+1}}. \quad (\text{A15})$$

In the limit as $\lambda \rightarrow \infty$ the Fourier transform will approach the value:

$$F(f) = (-i)^{k+1} (2\pi f)^{-(k+1)} \quad (\text{A16})$$

and the power density spectrum will approach the power-law form:

$$P(f) = (2\pi f)^{-2(k+1)}. \quad (\text{A17})$$

The full ensemble averaged PDS will be given by:

$$P(f) = \frac{\sigma_\epsilon^2}{(2\pi f)^m} \quad (\text{A18})$$

where σ_ϵ^2 is the mean power level of the underlying white noise (equal to the noise strength S) and $m = 2(k + 1)$ is the power-law spectral index. Now equation A5 can be viewed as a general formula for producing power-law noise by the convolution of a step $t^k H(t)$ with a white noise process.

A.1. Time Domain Properties

In practice, any physically realizable red noise time series will first be observed at a time $t = 0$ and have started at this or some earlier time. The linearity of the convolution integral allows the time series to be divided into the form:

$$r_m(t) = \frac{1}{k!} \int_T^0 (t - t')^k \epsilon(t') dt' + \frac{1}{k!} \int_0^t (t - t')^k \epsilon(t') dt' \quad (\text{A19})$$

where T can range to $-\infty$ and $m = 2(k + 1)$. The first integral referring to the past will contribute a smooth function to the time series after $t = 0$. Note that in this form, $r_m(t)$ is divided into two nonstationary processes. When $\epsilon(t)$ is viewed as a series of discrete impulses the time series $r_m(t)$ can be viewed as an accumulation of “steps” of the form $s(t) = t^k H(t)$. The smooth function will have a form related to that of an individual step. If the index k is a positive integer, the smooth function will have the form of a simple polynomial. For the random walk, $k=0$ ($1/f^2$ noise), the time series consists of a series of randomly ascending or descending “stair steps” of variable amplitude and duration. The smooth function will be a constant:

$$\int_T^0 \epsilon(t') dt' = C_0. \quad (\text{A20})$$

For $k=1$ ($1/f^4$ noise), the time series consists of a series of connected linear segments (“ramps”) and the smooth function will be a linear trend:

$$\int_T^0 (t - t') \epsilon(t') dt' = t \int_T^0 \epsilon(t') dt' - \int_T^0 t' \epsilon(t') dt' = C_0 t - C_1 \quad (\text{A21})$$

and for $k = 2$ ($1/f^6$ noise), the time series consists of quadratically shaped segments and the smooth function will be a quadratic trend and so on. Note that a polynomial fit of an order $l \geq k$ will remove the smooth function component completely when k is an integer.

The ensemble averaged expectation and variance of power-law noise at a time t can be easily calculated. Each point of a power-law noise realization simply consists of a linear combination of white noise, so the statistics will be directly related to the white noise statistics. The expectation, $\langle r_m(t) \rangle$ will be given by:

$$\langle r_m(t) \rangle = \frac{1}{k!} \left\langle \int_{-\infty}^t (t - t')^k \epsilon(t') dt' \right\rangle = \langle \epsilon(t) \rangle \frac{1}{k!} \int_{-\infty}^t (t - t')^k dt'. \quad (\text{A22})$$

If the times series is divided into two finite portions as in A19 and $k \neq -1$ the expectation has the simple form:

$$\langle r_m(t) \rangle = \frac{\langle \epsilon(t) \rangle}{(k + 1)!} (t + T)^{k+1}. \quad (\text{A23})$$

A zero mean white noise process implies that $\langle r_m(t) \rangle = 0$ as well.

The variance of $r_m(t)$ as a function of time, $\langle r_m(t)^2 \rangle - \langle r_m(t) \rangle^2$ can be calculated from:

$$\begin{aligned} \langle r_m(t)^2 \rangle &= \left(\frac{1}{k!} \right)^2 \left\langle \left(\int_{-\infty}^t (t - t')^k \epsilon(t') dt' \right)^2 \right\rangle \\ &= \left(\frac{1}{k!} \right)^2 \int_{-\infty}^t \int_{-\infty}^t (t - t')^k (t - t'')^k \langle \epsilon(t') \epsilon(t'') \rangle dt' dt'' \end{aligned}$$

$$\begin{aligned}
&= \left(\frac{1}{k!}\right)^2 \int_{-\infty}^t (t-t')^{2k} \langle \epsilon(t')^2 \rangle dt' \\
&= \left(\frac{\sigma_\epsilon}{k!}\right)^2 \int_{-\infty}^t (t-t')^{2k} dt'
\end{aligned} \tag{A24}$$

where use is made of the fact that for white noise:

$$\langle \epsilon(t')\epsilon(t'') \rangle = \sigma_\epsilon^2 \delta(t' - t'') \tag{A25}$$

where $\delta(t)$ is the Dirac delta-function. Note that the variance $\langle r_m(t)^2 \rangle$ at time t is in fact infinite for all values of k . If the time series is divided into two finite portions as in A19 with zero mean white noise being used and $k \neq -0.5$, the variance is finite and reduces to the simple expression:

$$\langle r_m(t)^2 \rangle = \frac{1}{(2k+1)} \left(\frac{\sigma_\epsilon}{k!}\right)^2 (t+T)^{2k+1}. \tag{A26}$$

Therefore, if one could measure $\langle r_m(t)^2 \rangle$ in this way, by averaging over a number of noise realizations for example, the PDS spectral index $m = 2(k+1)$, and the underlying white noise variance σ_ϵ^2 could be estimated in a straight forward manner.

The autocovariance can also be derived in a similar manner. The autocovariance is, for $\langle r_m(t) \rangle = 0$, given by:

$$\langle r_m(t)r_m(t+\tau) \rangle = \left(\frac{1}{k!}\right)^2 \left\langle \left(\int_{-\infty}^t (t-t')^k \epsilon(t') dt' \right) \left(\int_{-\infty}^{t+\tau} (t+\tau-t')^k \epsilon(t') dt' \right) \right\rangle. \tag{A27}$$

This expression reduces to:

$$\langle r_m(t)r_m(t+\tau) \rangle = \left(\frac{\sigma_\epsilon}{k!}\right)^2 \left(\int_{-\infty}^t (t-t')^k (t+\tau-t')^k dt' \right) \tag{A28}$$

with $\tau \geq 0$. Note that the autocovariance function depends on both the current time t as well as the lag τ . The Fourier transform of the autocovariance function has the form:

$$\int_{-\infty}^{\infty} e^{-i2\pi f\tau} \langle r_m(t)r_m(t+\tau) \rangle d\tau \tag{A29}$$

The exponential can be broken into the two terms $e^{-i2\pi f\tau} = e^{-i2\pi f(\tau-(t'-t))} e^{-i2\pi f(t'-t)}$ and after rearranging, the integral divides into two terms, one of the form A10 and one of its conjugate that can be solved in the limit as in A13. The Fourier transform will, in the limit, approach the power-law form given by A18.

Expression A27, after removing the past smooth function, has the form:

$$\langle r_m(t)r_m(t+\tau) \rangle = \left(\frac{\sigma_\epsilon}{k!}\right)^2 \left(\int_0^t (t-t')^k (t+\tau-t')^k dt' \right) \tag{A30}$$

which reduces to A24 when $\tau = 0$. For the three cases in which $k=0, 1$ and 2 , i.e. for $1/f^2$, $1/f^4$ and $1/f^6$ PLN this expression has the following forms:

For $k=0$:

$$\langle r_2(t)r_2(t+\tau) \rangle = \sigma_\epsilon^2 t \quad (\text{A31})$$

for $k=1$:

$$\langle r_4(t)r_4(t+\tau) \rangle = \frac{1}{6}\sigma_\epsilon^2 t^2 (2t + 3\tau) \quad (\text{A32})$$

and for $k=2$:

$$\langle r_6(t)r_6(t+\tau) \rangle = \frac{1}{120}\sigma_\epsilon^2 t^3 (6t^2 + 15t\tau + 10\tau^2) \quad (\text{A33})$$

Note the time dependence of the autocovariance for $r_4(t)$ and $r_6(t)$ after removal of the past smooth function. When the substitutions $t = t_<$ and $t + \tau = t_>$ are used then A31, A32 and A33 are seen to be the continuous white noise version of equations (23), (38) and (43) derived by Groth (1975b).

A.2. Discrete Red Power-law Noise

Any realizable red PLN process, in addition to being of limited duration, will be composed of steps of a finite size occurring at a finite rate. We now consider a discrete model of red PLN that is useful for generation of actual samples with Monte-Carlo routines. A discrete form of (A5) can be obtained by replacing $\epsilon(t)$ with the discrete white noise form:

$$\epsilon(t) = \sum_{j=-\infty}^{\infty} \epsilon_j \delta(t_j) \quad (\text{A34})$$

which produces the discrete power-law noise process:

$$\hat{r}_m(t) = \frac{1}{k!} \sum_{j=-\infty}^{j_{max}} (t - t_j)^k H(t - t_j) \epsilon(t_j) \quad (\text{A35})$$

where the power-law spectral index $m = 2(k + 1)$ and $H(t)$ is the unit step function as defined previously. The last white noise “event” in the time-series, $\epsilon(t_j)$, occurs at a time $t_{j_{max}}$ such that $t_{j_{max}} \leq t < t_{j_{max}+1}$. We choose the duration between events $\Delta t = t_j - t_{j-1}$ to be a random variable with a probability density function: $p(\Delta t) = R_g e^{-R_g \Delta t}$, i.e. the “waiting time” distribution of the Poisson process. The $\epsilon(t_j)$ are drawn from a discrete zero mean gaussian white noise process with a variance $\sigma_\epsilon^2(\Delta t_g) = \Delta t_g \sigma_\epsilon^2$ and a mean rate of step generation $R_g = \frac{1}{\Delta t_g}$ such that $\Delta t_g = \langle \Delta t \rangle$ (a noise process sometimes referred to as *white Poisson impulse noise*). The noise strength is given by $S = R_g \sigma_\epsilon^2(\Delta t_g)$ and along with the index k and R_g completely specify the type of noise process. Processes with the same noise

strength can be made by the frequent accumulation of many small steps or with fewer, larger steps in the same time interval.

The physical units of S depend on the units of $\hat{r}_m(t)$ and the specific power-law. For example, let $\hat{r}_m(t)$ be noise in the rotation phase of a pulsar so the physical units are cycles and let time be given in seconds. Then the units of $\epsilon(t_j)$ will be cycles sec^{-k} . Because $\sigma_\epsilon(\Delta t_g) = \sqrt{\frac{S}{R_g}}$ the units of S are $\text{cycles}^2 \text{sec}^{-(1+2k)}$. If $\hat{r}_m(t)$ is noise in the rotation frequency then the units of $\epsilon(t_j)$ will be Hz sec^{-k} and the units of S will be $\text{Hz}^2 \text{sec}^{-(1+2k)}$. If noise in the rotation frequency derivative then S will have units of $(\text{Hz/sec})^2 \text{sec}^{-(1+2k)}$, etc.

Any physical or simulated time-series will begin at a time that we can arbitrarily set at $t = 0$. Then $\hat{r}_m(t)$ will have the form:

$$\hat{r}_m(t) = \frac{1}{k!} \sum_{j=0}^{j_{max}} (t - t_j)^k H(t - t_j) \epsilon(t_j). \quad (\text{A36})$$

In this form it can be seen that $\hat{r}_m(t)$ is simply a generalization of the discrete PLN models contained in Groth (1975b), in which $k=0, 1, \text{and } 2$ correspond to his phase, frequency and slow-down noise definitions respectively. We can also rewrite $\epsilon(t_j)$ as a scaled version of a unit variance time-series $\epsilon_u(t_j)$ such that: $\epsilon(t_j) = \sqrt{S\Delta t_g} \epsilon_u(t_j)$ where $\sigma_{\epsilon_u}^2(\Delta t_g) = 1$. Equation (A35) then becomes:

$$\hat{r}_m(t) = \frac{\sqrt{S\Delta t_g}}{k!} \sum_{j=0}^{j_{max}} (t - t_j)^k H(t - t_j) \epsilon_u(t_j). \quad (\text{A37})$$

and is useful for generating discrete noise realizations of noise strength S . Now if $\hat{r}_m(t)$ above is used in its entirety to represent a power-law noise realization, the low frequency power contributed by the past will be too small so for an accurate representation, a sufficiently long portion of the early time series needs to be discarded.

Following Groth (1975b), we now derive the mean $\langle \hat{r}_m(t) \rangle$ and autocovariance $\langle \hat{r}_m(t) \hat{r}_m(t + \tau) \rangle$ for equation (A36). Now $\langle \hat{r}_m(t) \rangle$ is given by:

$$\begin{aligned} \langle \hat{r}_m(t) \rangle &= \left\langle \frac{1}{k!} \sum_{j=0}^{j_{max}} (t - t_j)^k H(t - t_j) \epsilon(t_j) \right\rangle \\ &= \frac{1}{k!} \sum_{j=0}^{j_{max}} \langle (t - t_j)^k H(t - t_j) \rangle \langle \epsilon(t_j) \rangle \\ &= \frac{\langle \epsilon(t) \rangle}{k!} \sum_{j=0}^{j_{max}} \langle (t - t_j)^k H(t - t_j) \rangle \end{aligned}$$

$$\begin{aligned}
&= \frac{\langle \epsilon(t) \rangle}{k!} R_g \int_0^t (t - t')^k dt' \\
&= \frac{\langle \epsilon(\Delta t_g) \rangle}{(k+1)!} t^{k+1} \quad (k \neq -1)
\end{aligned} \tag{A38}$$

where $\langle \epsilon(\Delta t_g) \rangle$ is the mean on a time-scale $\Delta t_g = R_g^{-1}$. This is the same equation as (A23) and when $k=0, 1$, and 2 reduces to Groth's results for phase, frequency and slow-down noise.

The autocovariance is given by:

$$\begin{aligned}
\langle \hat{r}_m(t) \hat{r}_m(t + \tau) \rangle &= \left\langle \left(\frac{1}{k!} \sum_{j=0}^{j_{max}} (t - t_j)^k H(t - t_j) \epsilon(t_j) \right) \left(\frac{1}{k!} \sum_{j=0}^{j_{max}+l} (t + \tau - t_j)^k H(t + \tau - t_j) \epsilon(t_j) \right) \right\rangle \\
&= \left(\frac{1}{k!} \right)^2 \sum_{j=0}^{j_{max}} \sum_{j'=0}^{j_{max}+l} \langle (t - t_j)^k (t + \tau - t_{j'})^k H(t - t_j) H(t + \tau - t_{j'}) \rangle \langle \epsilon(t_j) \epsilon(t_{j'}) \rangle \\
&= \left(\frac{\sigma_\epsilon(\Delta t_g)}{k!} \right)^2 \sum_{j=0}^{j_{max}} \langle (t - t_j)^k (t + \tau - t_j)^k H(t - t_j) H(t + \tau - t_j) \rangle \\
&= R_g \left(\frac{\sigma_\epsilon(\Delta t_g)}{k!} \right)^2 \int_0^t (t - t')^k (t + \tau - t')^k dt'
\end{aligned} \tag{A39}$$

where $t_{j_{max}} \leq t < t_{j_{max}+1}$ and $t_{j_{max}+l} \leq t + \tau < t_{j_{max}+l+1}$. The autocovariances derived by Groth (1975b) for his phase, frequency and slow-down noise definitions ($k=0, 1$ and 2 respectively) can be obtained from equation (A39) by the substitutions $t_{>} = t + \tau$ in the second term in the integral and $t_{<} = t$ elsewhere.

B. Generation of Red Power-Law Noise Using a Modified Timmer-König Method

A method for simulating power-law noise realizations has been proposed by Timmer & König (1995). Real and imaginary values of the Fourier amplitudes corresponding to a set of discrete Fourier frequencies are generated from a zero mean gaussian distribution and then weighted by a chosen Fourier frequency dependent power-law. The amplitudes are then Fourier transformed into the time-domain to generate a uniformly sampled time-series. A normalization for a particular noise strength is not given in their paper. We present below, in a recipe form, a modification of this method that can be used to generate power-law noise realizations with noise strength S .

To generate a power-law noise realization with N points we created two zero mean unit

variance gaussian white noise vectors x_j and y_j , $j = 0, 1 \dots N - 1$ and a corresponding weighting vector $w_j = (\frac{1}{j})^{\frac{m}{2}}$ where m is the desired power-law index. For the conventions used below, we assume that N is an even integer. We then formed a complex vector of Fourier amplitudes $r = A[0, (w_j x_j, w_j y_j), (w_{N-1-j} x_{N-1-j}, w_{N-j-1} y_{N-1-j})^*]$ where the first member of a complex pair $(w_j x_j, w_j y_j)$ is real and the second imaginary and the asterisk indicates a complex conjugate. The third set of terms contains the negative Fourier frequencies in which $j = 1 \dots N - 1$, while for the second set of positive Fourier frequencies, $j = 0 \dots N - 1$, so that the complex vector r contains a total of $2N$ terms. The Nyquist term was made purely real so that $y_{N-1} = 0$. The normalization constant $A = (SN)^{\frac{1}{2}} (\frac{N}{\pi})^{\frac{m}{2}}$ and was chosen so that the generated realization has an average noise strength S . A realization was then generated as a time series via the discrete inverse Fourier transform:

$$R(t_k) = \frac{1}{2N} \sum_{l=0}^{2N-1} r_l e^{\frac{-i\pi l k}{N}} \quad k = 0, 1, \dots, 2N - 1. \quad (\text{B1})$$

While $R(t_k)$ is a time-series of N independent points, only the first $N/2$ should be used. The autocorrelation function of the times-series produced by equation B1 is approximately correct for lags less than $N/2$, but is wrong for larger lags. This is due to the cyclic nature of the discrete Fourier transform, which treats the last point as the nearest neighbor of the first. Use of the full time series results in an under representation of low frequency power. Further discussion can be found in section 7 of this paper.

REFERENCES

- Alpar, A. M., Nandkumar, R. & Pines, D., 1986, ApJ, 311, 197
- Alpar, A. M., 2001, ApJ, 554, 1245
- Bildsten, L., et al., 1997, ApJS, 113, 367
- Boynton, P. E., Groth, E. J., Hutchinson, D. P., Nanos, Jr., G. P., Partridge, R. B., & Wilkinson, D. T., 1972, ApJ, 175, 217
- Boynton, P. E., 1981, in IAU Symposium 95, Pulsars, ed. R. Wielebinski and W. Seiber (Dordrecht:Reidel), p. 279
- Cheng, K. S., 1987, ApJ, 321, 805
- Cordes, J. M., 1980, ApJ, 237, 216
- Cordes, J. M. & Downs, G. S., 1980, ApJS, 59, 343
- D'Alessandro, F., 1997, Ap&SS, 246, 73

- Deeter, J., 1981, PhD Thesis, Univ. of Washington
- Deeter, J., 1984, ApJ, 281, 482
- Deeter J. E., & Boynton P. E., 1982, ApJ, 261, 337
- Deshpande, A. A., D’Alessandro, F., & McCulloch, P. M., 1996, J. Astrophys. Astr., 17, 7
- Gavriil, F. P., Kaspi, V. M. & Woods, P. M., 2002, Nature, 419, 142
- Groth, E., 1975a, ApJS, 29, 431
- Groth, E., 1975b, ApJS, 29, 443
- Groth, E., 1975c, ApJS, 29, 453
- Gullahorn, G. E., Isaacman, R., Rankin, J. M. & Payne, R. P., 1977, AJ, 82, 309
- Harris, F. Proc. of IEEE, 66, 51
- Hulleman, F., van Kerkwijk, M. H. & Kulkarni, S. R., 2000, Nature, 408, 689
- Israel, G. L., Covino, S., Stella, L., Campana, S., Marconi, G., Mignani, R., et al., 2002, ApJ, 580, L143
- Konacki, M., Lewandowski, W., Wolszczan, A., Doroshenko, O., & Kramer, M., 1999, ApJ, 519, L81-84
- Lin, D., Woosley, S. E. & Bodenheimer, P., 1991, Nature, 383, 827
- Lohsen, E. H. G., 1981, A&AS, 44, 1
- Lyne A. G. & Pritchard R. S., 1987, MNRAS, 229, 223
- Lyne A. G., Pritchard R. S. & Smith F. G., 1988, MNRAS, 229, 223
- Lyne A. G., Pritchard R. S. & Smith F. G., 1993, MNRAS, 265, 1003
- Lyne A. G., Smith F. G. & Pritchard R. S., Nature, 359, 706
- Manchester, R. N. & Taylor, J. H., 1997, “Pulsars” W.H. Freeman and Company, San Francisco, p. 101
- Mereghetti, S., Chiarlone, L., Israel, G. L., & Stella, L., 2002, in Neutron Stars, Pulsars and Supernova Remnants, ed. W. Becker, H. Lesch, & J. Trümper (MPE Rep. 278: MPE), 29 (astro-ph/02051221)
- Press, W. H., Teukolsky, S. A., Vetterling, W. T., & Flannery, B. P., “Numerical Recipes in Fortran”, 2nd ed., Cambridge University Press, Cambridge, UK, p. 569
- Stairs, I. H., Lyne, A. G., & Shemar, S., L., 2000, Nature, 406, 484
- Timmer, J., & König, M., 1995, A&A, 300, 707

Weisskopf, M., Hester, J., Tennant, A., et al., 2000, ApJ, 536, L81

Fig. 1.— Top: Crab arrival time residuals obtained from radio observations by Jodrell Bank after removal of a quartic polynomial and correcting for dispersion effects. Middle: Power spectrum of the frequency derivative computed from the above residuals using the Deeter polynomial method (solid circles). Measurement noise power is shown by the triangles. Bottom: Deeter polynomial power spectrum (solid circles) after dividing by $2\pi f$. The measurement noise power (triangles) has been similarly corrected. The histogram displays the windowed power spectrum of the arrival time residuals displayed in the top panel using a Hann window with $\alpha = 2$.

Fig. 2.— Examples of discrete red-noise time series showing resolved steps. The number on the far right gives the power-law index of the process. The bottom time series shows the discrete white noise realization from which the red-noise time series were generated.

Fig. 3.— Sample of red noise realizations of increasing redness generated from the same underlying white noise realization (left panel set). The power-law index, m , for $1/f^m$ noise is given in the inset on each left panel set. The right panel set shows the same realizations after detrending by a cubic polynomial fit.

Fig. 4.— Top: Example of a cubic polynomial detrended $1/f^3$ noise realization with a noise strength $S = 1 \times 10^{-6}$ cycles²/day² (approximately equal to the Crab pulsar) generated using the time-domain method. Middle: Hann windowed ($\alpha = 2$) power density spectrum (PDS) showing power-law slope of -2.998 ± 0.077 from fit to power between vertical dashed lines. For comparison, the smoother curve offset above is an average PDS of 1024 identically generated realizations. Bottom: Flattened PDS after multiplication by $(2\pi f)^3$, where f is frequency. The smoother average flattened PDS is also shown offset above where the highest frequency power exhibits an increase by $2\times$ due to aliasing.

Fig. 5.— Averages of 1024 flattened power spectra for power-law noise realizations of unit strength. A high frequency sinusoid (visible as peak near $f = 0.1$ and white noise have been added to each realization. Power-law spectral index m shown to left of the flat lines that display the predicted pure power-law form for unit noise strength. Power spectra with $m > 2.0$ have been offset in power for display purposes, otherwise scale is the same. The average spectra of the white noise alone (for $f > 0.08$) is shown as the sloping lines. The lower spectra of each pair show average power spectra after realizations have been detrended by cubic polynomials.

Table 1. Crab pulse phase ephemeris

Parameter	Value
$t_0(MJD)$	45395.94232638889
$\phi_0(cycles)$	4.445(6)
$\nu_0(Hz)$	30.04669082632(13)
$\dot{\nu}_0(10^{-10} Hz s^{-1})$	−3.80599313(13)
$\ddot{\nu}_0(10^{-20} Hz s^{-2})$	1.214636(13)
$\ddot{\nu}_0(10^{-30} Hz s^{-3})$	−1.425(16)

Table 2. Fitted Cosine parameters

Parameter	Value
$t_0(MJD)$	46390.0
$A(cycles)$	0.23 ± 0.03
$B(cycles)$	0.12 ± 0.03
$\Phi_0(radians)$	1.09 ± 0.116
$P(days)$	568 ± 10
$A_0(cycles)$	0.26 ± 0.03

Fig. 6.— Top: Crab arrival time residuals obtained from radio observations by Jodrell Bank after removal of a quartic polynomial, correcting for dispersion effects *and* interpolating onto a uniform grid. Middle: Hann windowed ($\alpha = 1$) power density spectrum showing power-law slope of -3.09 ± 0.05 from fit to power between vertical dashed lines (frequency range 0.003 – 0.1 cycles/day). Horizontal line shows calculated power level of statistical measurement noise. Bottom: flattened PDS after multiplication by $(2\pi f)^3$, where f is frequency. Note the highly significant peak at $f = 0.0018$ cycles/day. Mean power level (between vertical dashed lines) is $9.26(0.50) \times 10^{-7}$ cycles²/day². Solid vertical line shows cosine frequency from table 2.

Fig. 7.— Top: The numerical 1st derivative of the uniformly binned spline fit to the Crab timing residuals. The superposed sinusoid is the derivative of the sinusoid fit to the Crab timing phase residuals. Middle: A closeup of the Crab timing residuals at the time of the small glitch occurring at $\text{JD} - 2440000.5 = 6664$. The raw measurements are plotted in top, the spline interpolation underneath. Errors are plotted for the raw measurements but are generally smaller than the symbol size. Bottom: A similar closeup of the region associated with the first large excursion in the numerical 1st derivative. A possible glitch may have occurred here.

Fig. 8.— Comparison of average power spectra computed using the Deeter polynomial method (diamonds with error bars) and windowed power spectra using a Hann window with $\alpha = 2$ of the same 32 uniformly sampled noise realizations. The noise is $1/f^3$ PLN generated using the time domain method and detrended by a cubic polynomial fit. The spectra have been flattened for the case of a $1/f^3$ power-law. High (top two spectra) and low (bottom three spectra) frequency sinusoids have been added to the noise realizations to show the effect of discrete features on the power spectrum estimation. The power spectra have been shifted in power for display purposes but the noise strength is the same in all cases.

Fig. 9.— Top: Crab pulsar optical timing pulse phase residuals from Groth (1975c) for period after 1969 glitch. Offset below is a cubic spline interpolation onto a uniform time series. Middle: Solid circles mark the Deeter polynomial power spectrum of the pulse frequency derivative (flat for $1/f^4$ noise in pulse phase). Triangles connected by dotted line mark computed measurement noise spectrum. Dashed line shows power level measured by Deeter (1981) in his analysis of these data. Bottom: Above PDS after multiplication by $(2\pi f)$, which assumes that the real spectrum is $1/f^3$ noise in pulse phase. Note the “bump” in the power near log frequency -3.0 . Dashed horizontal line shows noise power level measured from Jodrell Bank measurements. Solid vertical line marks a period of 568 days. Histogram shows Hann windowed power ($\alpha = 2$) power of spline interpolation flattened assuming an power-law index of -3 .

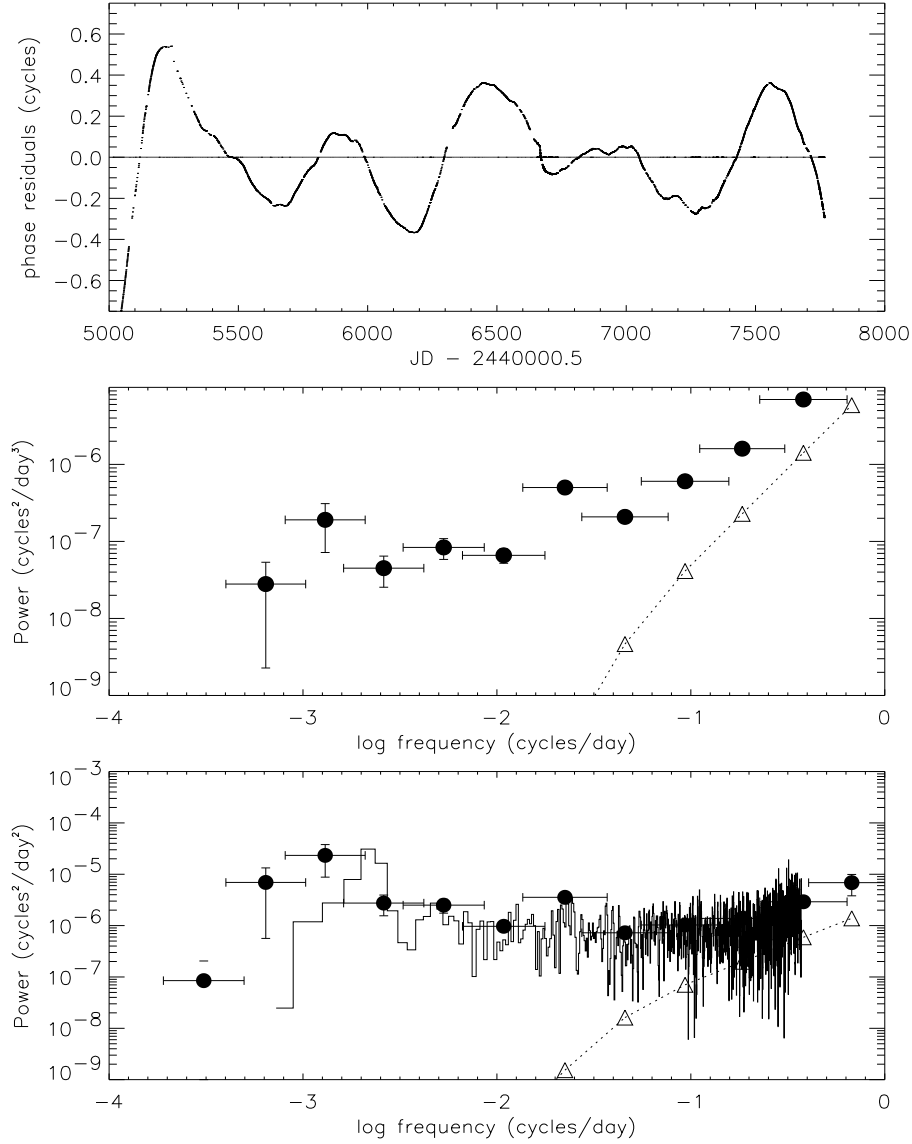


Fig 1. Top: Crab arrival time residuals obtained from radio observations by Jodrell Bank after removal of a quartic polynomial and correcting for dispersion effects. Middle: Power spectrum of the frequency derivative computed from the above residuals using the Deeter polynomial method (solid circles). Measurement noise power is shown by the triangles. Bottom: Deeter polynomial power spectrum (solid circles) after dividing by $2\pi f$. The measurement noise power (triangles) has been similarly corrected. The histogram displays the windowed power spectrum of the arrival time residuals displayed in the top panel using a Hann window with $\alpha = 2$.

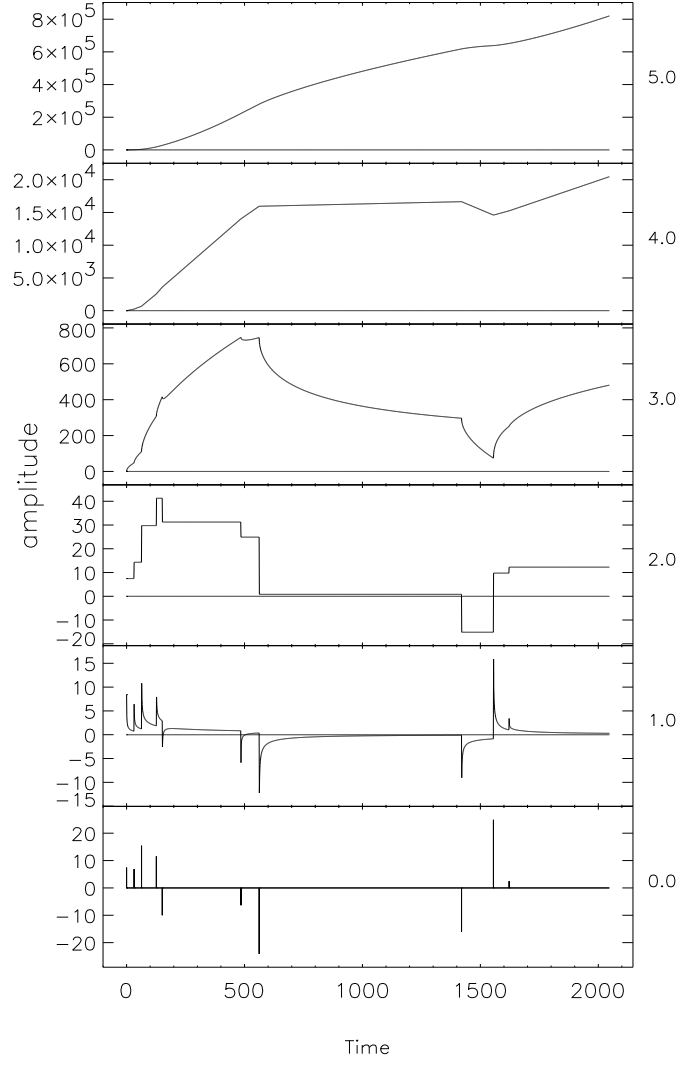


Fig 2. Examples of discrete red-noise time series showing resolved steps. The number on the far right gives the power-law index of the process. The bottom time series shows the discrete white noise realization from which the red-noise time series were generated.

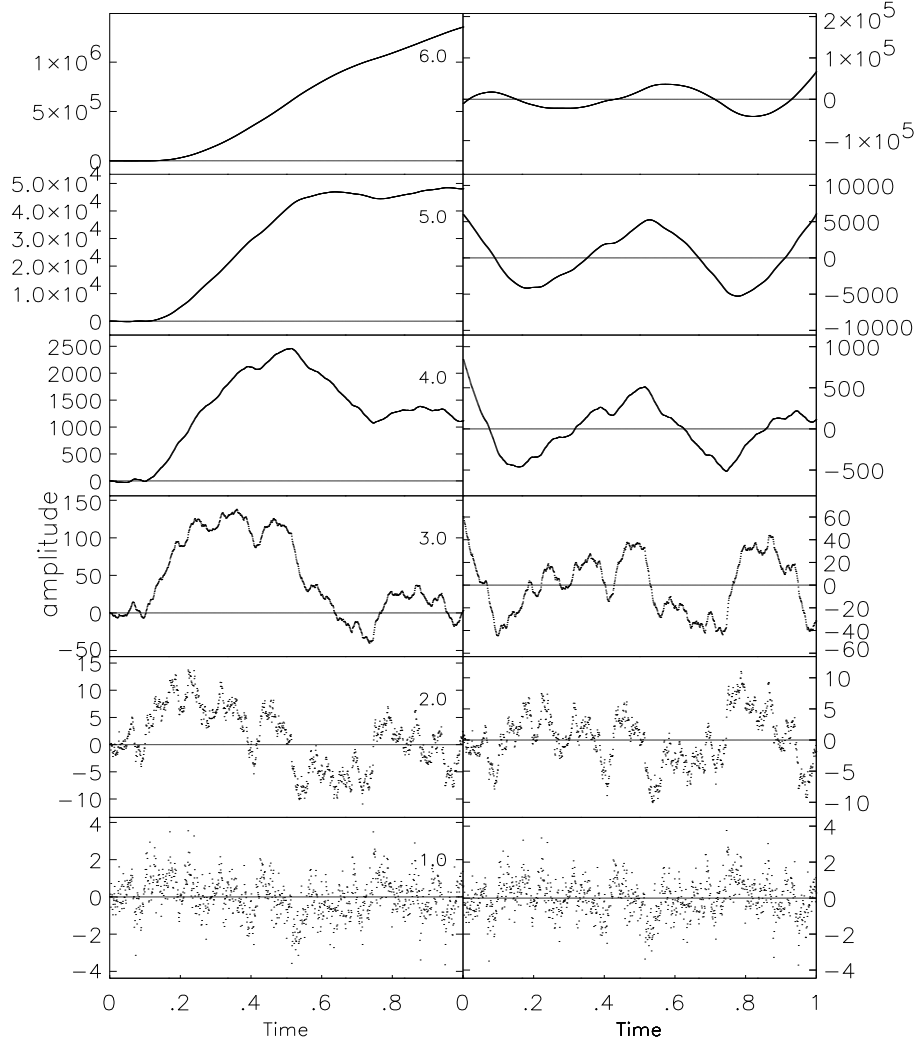


Fig 3. Sample of red noise realizations of increasing redness generated from the same underlying white noise realization (left panel set). The power-law index, m , for $1/f^m$ noise is given in the inset on each left panel set. The right panel set shows the same realizations after detrending by a cubic polynomial fit.

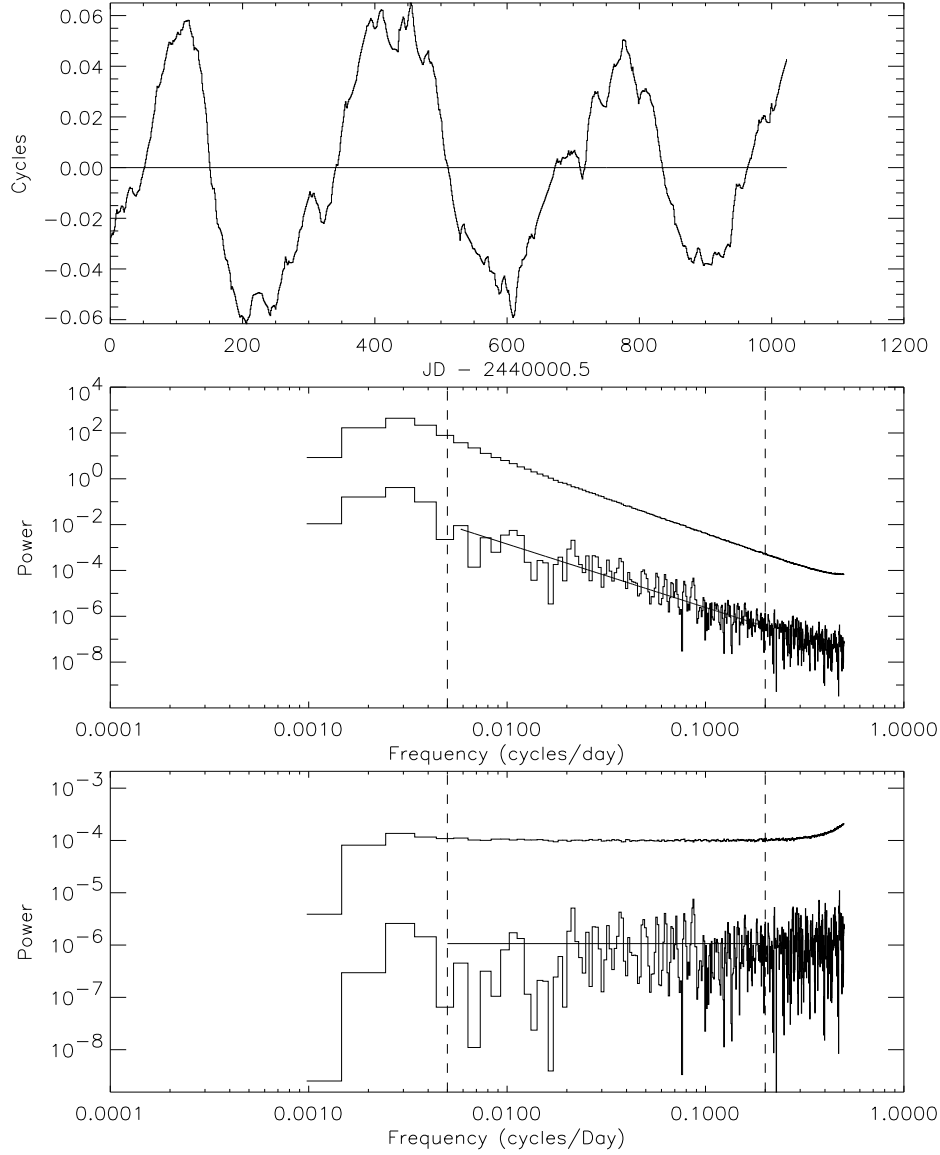


Fig 4. Top: Example of a cubic polynomial detrended $1/f^3$ noise realization with a noise strength $S = 1 \times 10^{-6}$ cycles²/day² (approximately equal to the Crab pulsar) generated using the time-domain method. Middle: Hann windowed ($\alpha = 2$) power density spectrum (PDS) showing power-law slope of -2.998 ± 0.077 from fit to power between vertical dashed lines. For comparison, the smoother curve offset above is an average PDS of 1024 identically generated realizations. Bottom: Flattened PDS after multiplication by $(2\pi f)^3$, where f is frequency. The smoother average flattened PDS is also shown offset above where the highest frequency power exhibits an increase by $2\times$ due to aliasing.

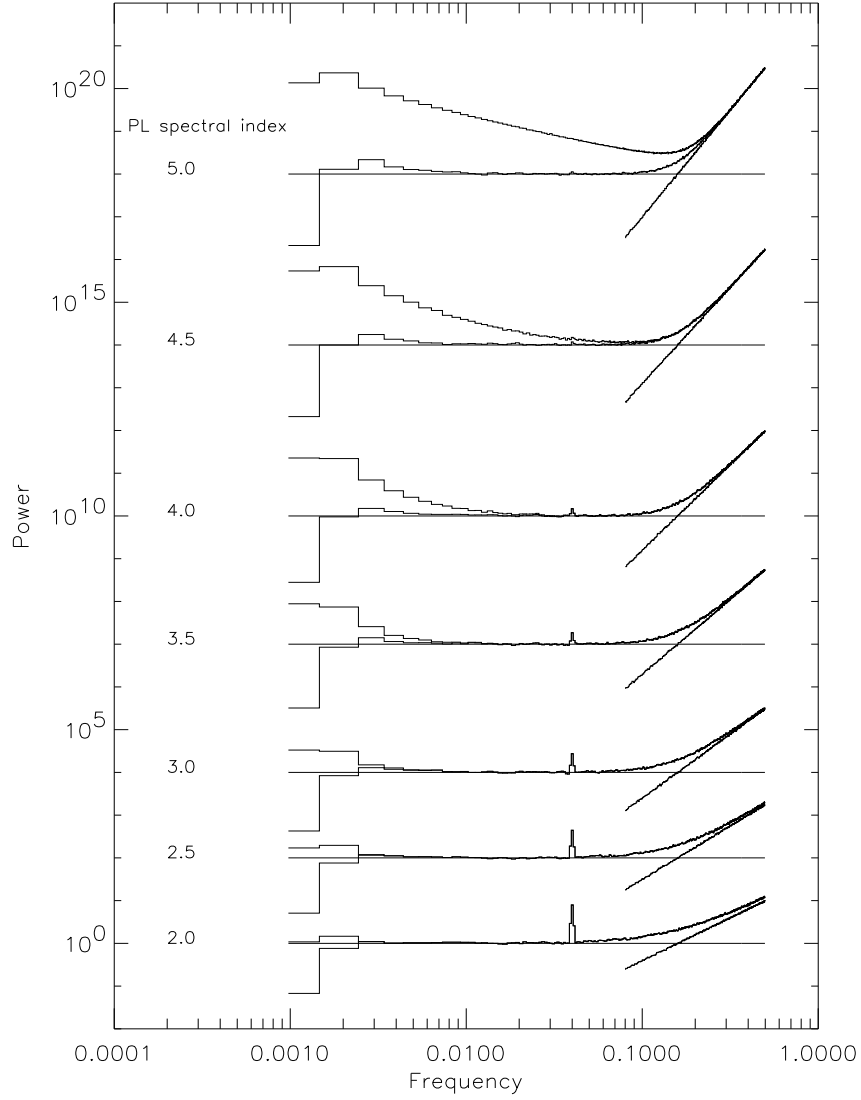


Fig 5. Averages of 1024 flattened power spectra for power-law noise realizations of unit strength. A high frequency sinusoid (visible as peak near $f = 0.1$ and white noise have been added to each realization. Power-law spectral index m shown to left of the flat lines that display the predicted pure power-law form for unit noise strength. Power spectra with $m > 2.0$ have been offset in power for display purposes, otherwise scale is the same. The average spectra of the white noise alone (for $f > 0.08$) is shown as the sloping lines. The lower spectra of each pair show average power spectra after realizations have been detrended by cubic polynomials.

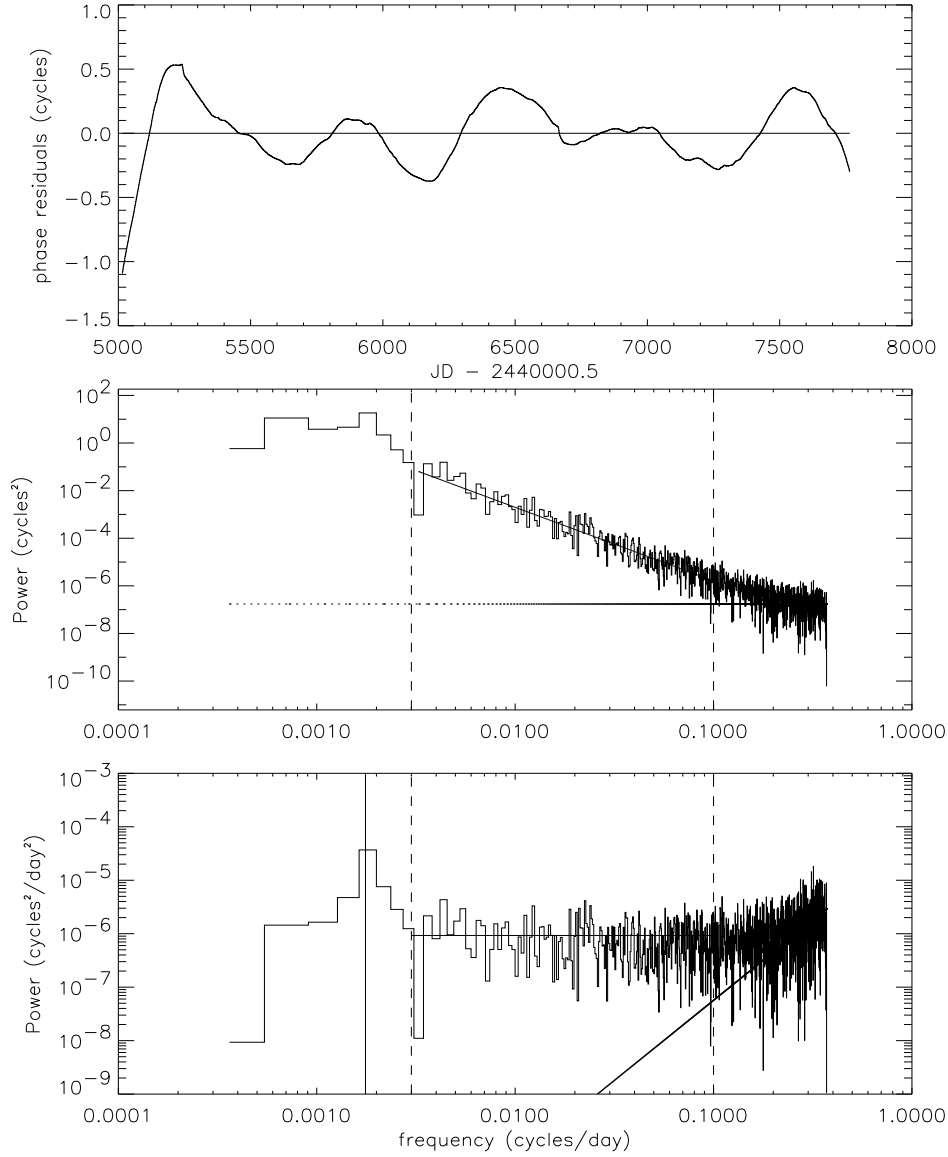


Fig 6. Top: Crab arrival time residuals obtained from radio observations by Jodrell Bank after removal of a quartic polynomial, correcting for dispersion effects *and* interpolating onto a uniform grid. Middle: Hann windowed ($\alpha = 1$) power density spectrum showing power-law slope of -3.09 ± 0.05 from fit to power between vertical dashed lines (frequency range 0.003 – 0.1 cycles/day). Horizontal line shows calculated power level of statistical measurement noise. Bottom: flattened PDS after multiplication by $(2\pi f)^3$, where f is frequency. Note the highly significant peak at $f = 0.0018$ cycles/day. Mean power level (between vertical dashed lines) is $9.26(0.50) \times 10^{-7}$ cycles²/day². Solid vertical line shows cosine frequency from table 2.

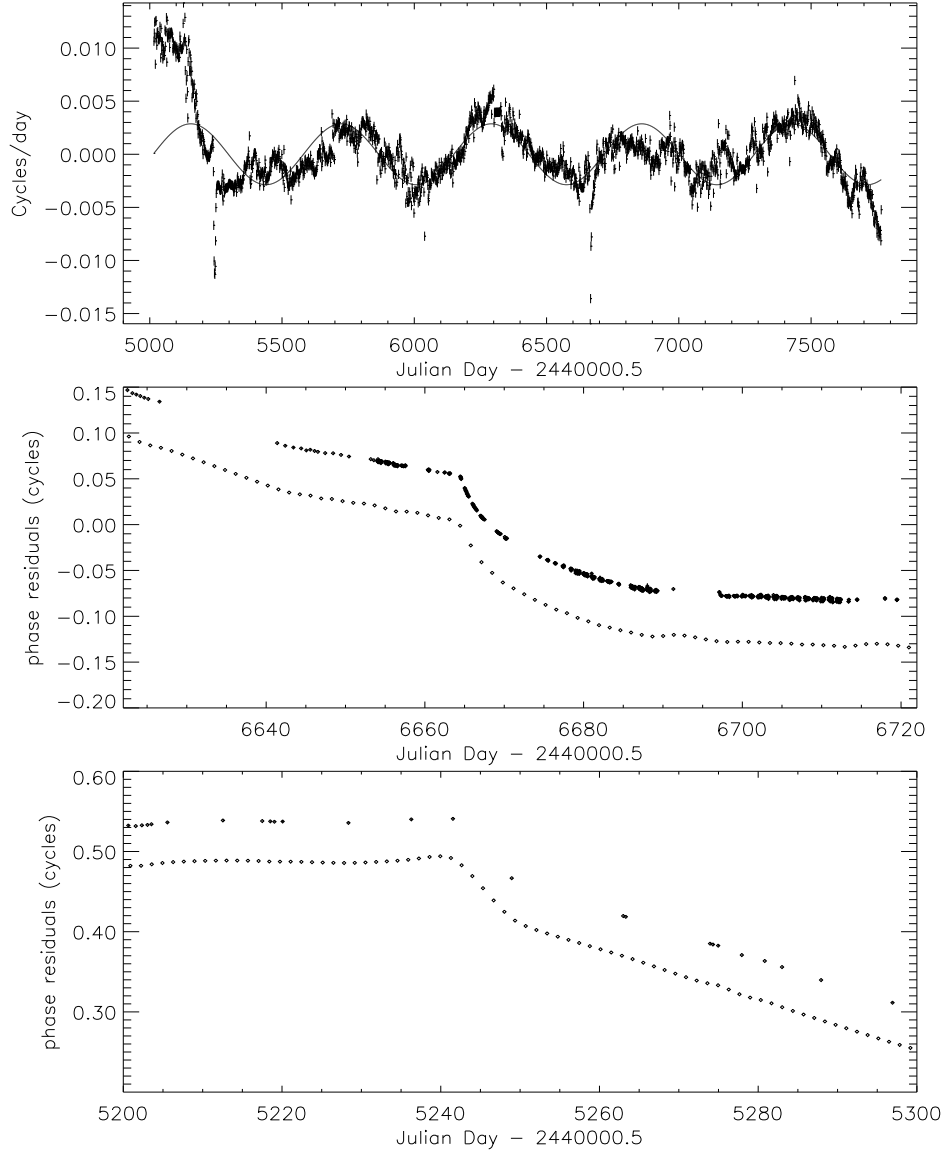


Fig 7. Top: The numerical 1st derivative of the uniformly binned spline fit to the Crab timing residuals. The superposed sinusoid is the derivative of the sinusoid fit to the Crab timing phase residuals. Middle: A closeup of the Crab timing residuals at the time of the small glitch occurring at $\text{JD} - 2440000.5 = 6664$. The raw measurements are plotted in top, underneath (diamonds) is the spline interpolation. Bottom: A similar closeup of the region associated with the first large excursion in the numerical 1st derivative. A possible glitch may have occurred here.

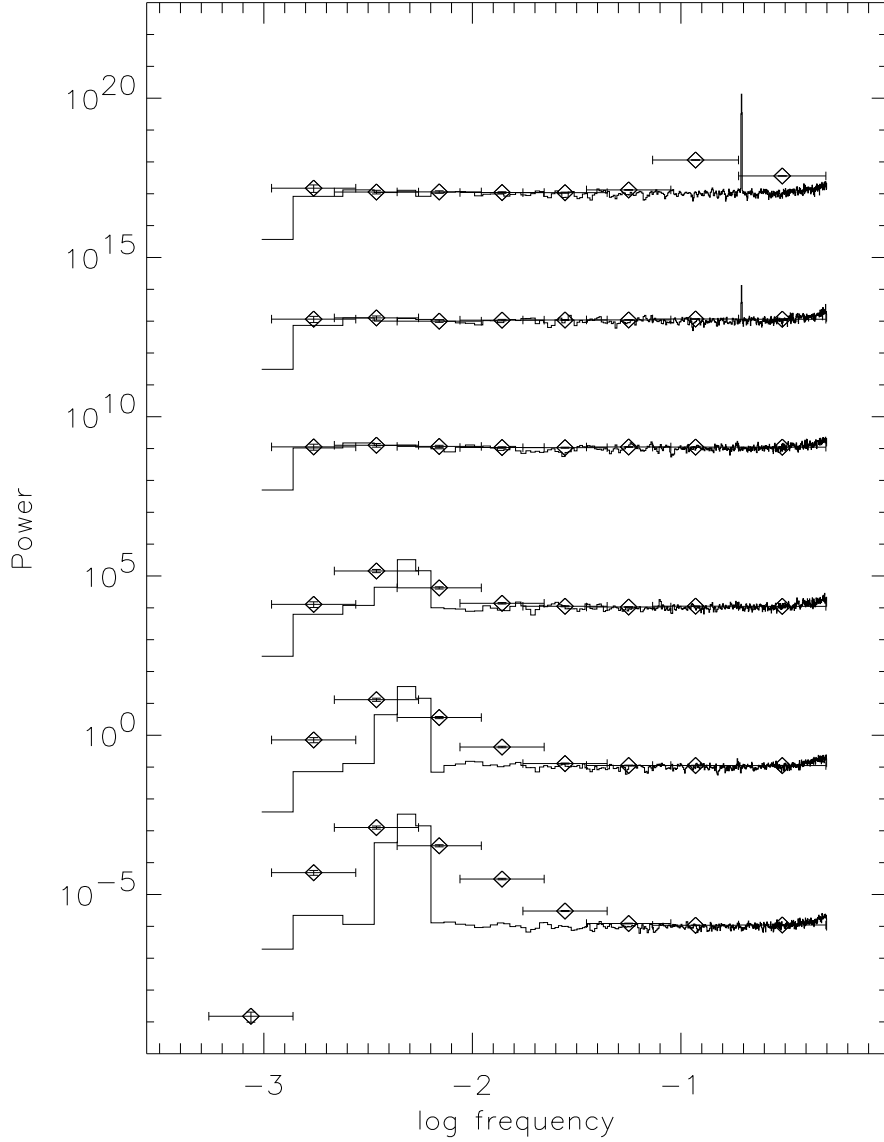


Fig 8. Comparison of average power spectra computed using the Deeter polynomial method (diamonds with error bars) and windowed power spectra using a Hann window with $\alpha = 2$ of the same 32 uniformly sampled noise realizations. The noise is $1/f^3$ PLN generated using the time domain method and detrended by a cubic polynomial fit. The spectra have been flattened for the case of a $1/f^3$ power-law. High (top two spectra) and low (bottom three spectra) frequency sinusoids have been added to the noise realizations to show the effect of discrete features on the power spectrum estimation. The power spectra have been shifted in power for display purposes but the noise strength is the same in all cases.

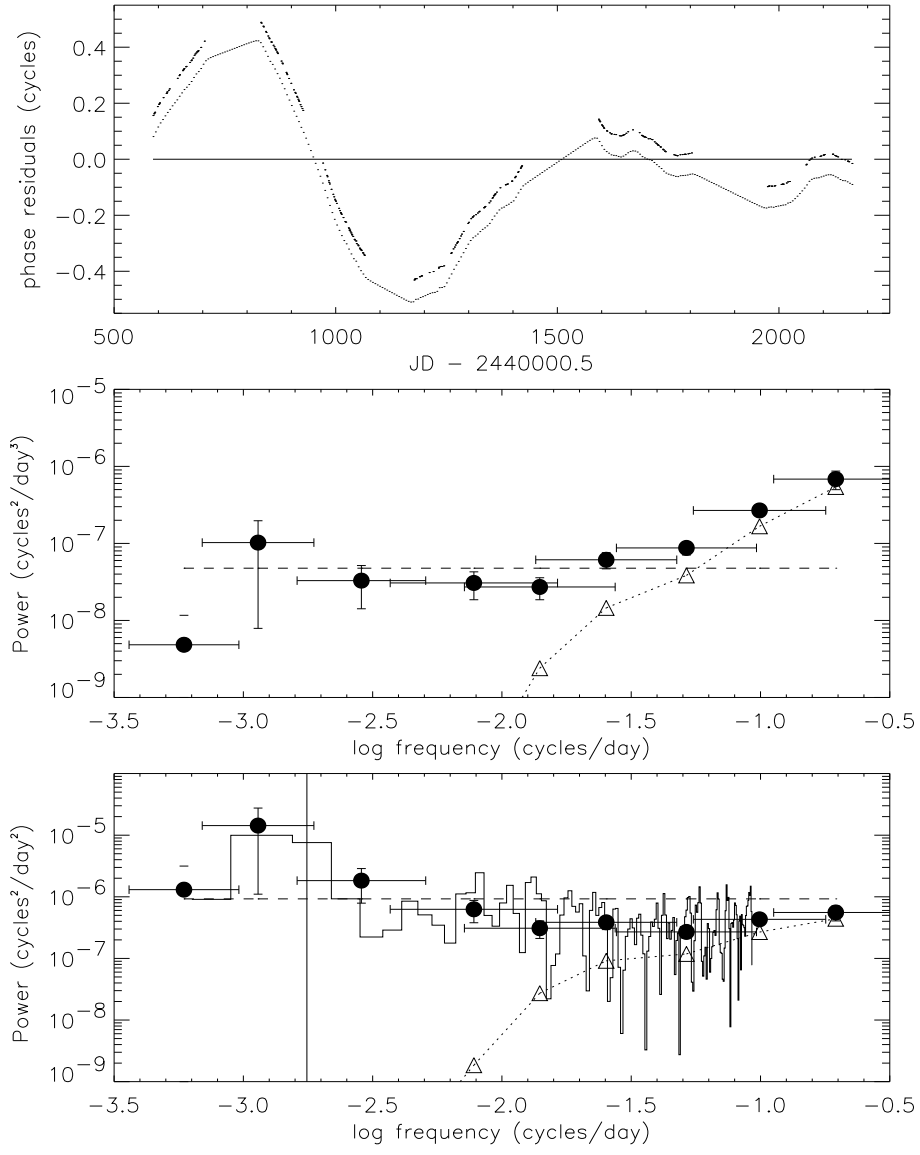


Fig 9. Top: Crab pulsar optical timing pulse phase residuals from Groth (1975c) for period after 1969 glitch. Offset below is a cubic spline interpolation onto a uniform time series. Middle: Solid circles mark the Deeter polynomial power spectrum of the pulse frequency derivative (flat for $1/f^4$ noise in pulse phase). Triangles connected by dotted line mark computed measurement noise spectrum. Dashed line shows power level measured by Deeter (1981) in his analysis of these data. Bottom: Above PDS after multiplication by $(2\pi f)$, which assumes that the real spectrum is $1/f^3$ noise in pulse phase. Note the “bump” in the power near log frequency -3.0 . Dashed horizontal line shows noise power level measured from Jodrell Bank measurements. Solid vertical line marks a period of 568 days. Histogram shows Hann windowed power ($\alpha = 2$) power of spline interpolation flattened assuming an power-law index of -3 .